THE ASTROPHYSICAL JOURNAL

An International Review of Spectroscopy and Astronomical Physics

FOUNDED IN 1895 BY GEORGE E. HALE AND JAMES E. KEELER

EDITORS

HENRY G. GALE
Ryerson Physical Laboratory of the University of Chicago

FREDERICK H. SEARES
Mount Wilson Observatory of the Carnegie Institution of Washington

OTTO STRUVE
Yerkes Observatory of the University of Chicago

COLLABORATORS

WALTER S. ADAMS, *Mount Wilson Observatory;* JOSEPH S. AMES, *Johns Hopkins University;* WILLIAM W. CAMPBELL, *Lick Observatory;* HENRY CREW, *Northwestern University;* CHARLES FABRY, *Université de Paris;* ALFRED FOWLER, *Imperial College, London;* EDWIN HUBBLE, *Mount Wilson Observatory;* HEINRICH KAYSER, *Universität Bonn;* ROBERT A. MILLIKAN, *Institute of Technology, Pasadena;* HUGH F. NEWALL, *Cambridge University;* FRIEDRICH PASCHEN, *Reichsanstalt, Charlottenburg;* HENRY N. RUSSELL, *Princeton University;* FRANK SCHLESINGER, *Yale Observatory;* HARLOW SHAPLEY, *Harvard College Observatory*

VOLUME 87

JANUARY–JUNE 1938

THE UNIVERSITY OF CHICAGO PRESS
CHICAGO, ILLINOIS

THE CAMBRIDGE UNIVERSITY PRESS, LONDON
THE MARUZEN COMPANY LIMITED, TOKYO
THE COMMERCIAL PRESS, LIMITED, SHANGHAI

PUBLISHED JANUARY, MARCH, APRIL, MAY,
JUNE 1938

COMPOSED AND PRINTED BY THE UNIVERSITY OF CHICAGO PRESS
CHICAGO, ILLINOIS, U.S.A.

Astron Obs
Wash

CONTENTS

NUMBER I

PAGE

NEW SOLUTIONS OF THE EQUATION OF RADIATIVE TRANSFER. Lyman Spitzer, Jr. 1

UNIDENTIFIED INTERSTELLAR LINES IN THE YELLOW AND RED. Paul W. Merrill and O. C. Wilson 9

RELATIVE *f*-VALUES FOR LINES OF *Fe* I AND *Ti* I. Robert B. King and Arthur S. King 24

TEMPERATURE IN THE SOLAR REVERSING LAYER DERIVED FROM TITANIUM LINES. Robert B. King 40

THE EFFECT OF AN ADIABATIC LAYER UPON SOLAR LIMB DARKENING. Philip C. Keenan 45

LINE INTENSITIES IN ULTRAVIOLET STELLAR SPECTRA. Lawrence H. Aller and Laurence G. Stoddard 53

THE FUNDAMENTAL ARC SERIES IN SODIUM AND ITS PRESENCE IN THE SUN. Paul Rood and R. A. Sawyer 68

NOTES 72

THE ORBIT OF b PERSEI. J. F. Heard (72). NOTE ON THE GLOBULAR CORONA. Dana K. Bailey (74). PHOTOELECTRIC MEASURES OF HD 199140. C. M. Huffer (76). NINE WHITE STARS OF LARGE PROPER MOTION. G. P. Kuiper and C. K. Seyfert (78). SOME NEW SPECTRA OF GALACTIC NEBULAE. Jesse L. Greenstein and L. G. Henyey (79).

NUMBER II

EQUIVALENT WIDTHS AND THE TEMPERATURE OF THE SOLAR REVERSING LAYER. Donald H. Menzel, James G. Baker, and Leo Goldberg . . 81

ULTRAVIOLET ABSORPTION SPECTRA OF SOME EARLY-TYPE STARS. Walter S. Adams and Theodore Dunham, Jr. 102

THE SPARK SPECTRUM OF IRON, λλ 5016–7712 WITH IDENTIFICATIONS OF *Fe* II LINES IN THE SOLAR SPECTRUM. Arthur S. King 109

STUDIES BASED ON THE INTENSITIES AND DISPLACEMENTS OF INTERSTELLAR LINES. Paul W. Merrill and Roscoe F. Sanford 118

THE SECONDARY VARIATION OF δ SCUTI. T. E. Sterne 133

A DETERMINATION OF SELECTIVE ABSORPTION BASED ON THE SPECTROPHOTOMETRY OF REDDENED B STARS. Jesse L. Greenstein 151

PAGE

AN IMPROVED DESCRIPTION OF THE THORIUM SPECTRUM. Mark Fred . 176

A NEW BAND IN THE ABSORPTION SPECTRUM OF THE EARTH'S ATMOSPHERE. Arthur Adel and C. O. Lampland 198

NOTES 204

ζ ORIONIS, A Be STAR. Ernest Cherrington, Jr. (204). A STAR MODEL WITH SELECTIVE THERMO-NUCLEAR SOURCE. G. Gamow (206). A SPECTROPHOTOMETRIC STUDY OF ε AURIGAE. John S. Hall (209). NOTE ON HALL'S MEASURES OF ε AURIGAE. G. P. Kuiper (213).

REVIEWS 216

NUMBER III

THE TOTAL LIGHT AND COLOR OF THE SOLAR CORONA OF JUNE 8, 1937. Joel Stebbins and A. E. Whitford 225

THE MAGNITUDES OF THE THIRTY BRIGHTEST STARS IN THE NORTH POLAR SEQUENCE. Joel Stebbins and A. E. Whitford 237

PHOTOELECTRIC MAGNITUDES AND THE INTERNATIONAL STANDARDS. Frederick H. Seares 257

COMPARISON OF LEIDEN AND MOUNT WILSON MAGNITUDES FOR POLAR STARS. Frederick H. Seares 280

POLARIZATION OF THE SOLAR CORONA IN THE TOTAL ECLIPSES OF 1932 AND 1934. Willi M. Cohn 284

ATOMIC LINES IN THE SPECTRUM OF ANTARES. Dorothy N. Davis . . 335

INVESTIGATION OF STANDARDS OF MAGNITUDE WITH A WEDGE PHOTOMETER. Alice H. Farnsworth 352

A STUDY OF THE GLOBULAR CLUSTER MESSIER 92. J. J. Nassau . . . 361

REVIEWS 367

NUMBER IV

GEORGE ELLERY HALE, 1868–1938. Walter S. Adams 369

A COMPARISON OF SPECTROSCOPIC AND TRIGONOMETRIC PARALLAXES. Henry Norris Russell and Charlotte E. Moore 389

THE PHOTOGRAPHIC DETERMINATION OF STELLAR PARALLAXES WITH THE 60- AND 100-INCH REFLECTORS. Adriaan van Maanen 424

ON THE POSSIBILITY OF DETECTING MOLECULAR HYDROGEN AND NITROGEN IN PLANETARY AND STELLAR ATMOSPHERES BY THEIR ROTATION-VIBRATION SPECTRA. Gerhard Herzberg 428

QUADRUPOLE ROTATION-VIBRATION SPECTRUM OF H_2. Hubert M. James and Albert Sprague Coolidge 438

ON THE DETERMINATION OF COLOR INDICES OF STARS FROM A CLASSIFICATION OF THEIR SPECTRA. W. W. Morgan 460

PAGE

Ionization and Recombination in the Theory of Stellar Absorption Lines and Nebular Luminosity. S. Chandrasekhar 476

Reviews 496

NUMBER V

Far Infrared Absorption of Atmospheric Water Vapor. Walter M. Elsasser 497

On the State of Matter in the Interior of the Planets. Rupert Wildt 508

Radial Velocities of Some Early-Type Stars. Roscoe F. Sanford and Paul W. Merrill 517

On the Helium and Hydrogen Content of the Interior of the Stars. Bengt Strömgren 520

An Integral Theorem on the Equilibrium of a Star. S. Chandrasekhar 535

The Eclipsing Variable Star μ' Scorpii. Paul Rudnick and C. T. Elvey 553

The 150-Foot Nebular Spectrograph of the McDonald Observatory. O. Struve, G. Van Biesbroeck, and C. T. Elvey 559

Evidence for Complex Structure in Lines of Interstellar Sodium. C. S. Beals 568

The Spectrum of γ Cassiopeiae in the Photographic Region. Ralph B. Baldwin 573

Notes 577

The Change of the Luminosity Function with Height above the Galactic Plane. Jesse L. Greenstein (577). The Colors of Reflection Nebulae. Jesse L. Greenstein (581). The Relation of the Brightness of the Night Sky to Zenith Distance. Jessie Rudnick (584). Atlas of the Spectrum of Nova Herculis 1934. F. J. M. Stratton (588). On the Spectral Types and Luminosities of the M Dwarfs. W. W. Morgan (589). Notes on Proper Motion Stars. G. P. Kuiper (592).

Index 597

THE ASTROPHYSICAL JOURNAL

AN INTERNATIONAL REVIEW OF SPECTROSCOPY AND ASTRONOMICAL PHYSICS

VOLUME 87 JANUARY 1938 NUMBER 1

NEW SOLUTIONS OF THE EQUATION OF RADIATIVE TRANSFER

LYMAN SPITZER, JR.

ABSTRACT

Solutions of the equation of radiative transfer are given for two assumed variations of η_ν with optical depth, valid for η_ν increasing or decreasing with τ. The first appears as a generalization of the Eddington solution. The second avoids the negative absorption inherent in previous investigations and leads to a simple formula convenient for numerical applications. For certain values of the constants the formulae are expressible in terms of simple powers and exponents.

Discussion of the equation of radiative transfer as applied to the formation of a spectral line has hitherto been limited almost entirely to the case in which η_ν, the ratio of the line and the continuous absorption coefficients, does not change with optical depth. Approximate treatments for small variations have recently been given by B. Strömgren,[1] and extensive numerical integrations for variable η_ν have been carried out by Pannekoek[2] and others. The only rigorous solution, however, has been given by Eddington[3] in the special case

$$\frac{1}{1+\eta_\nu} = a + b\tau ,$$

where τ is, as usual, the optical depth in the adjacent continuous spectrum.

It is of interest to note that rigorous solutions are available under a considerable variety of assumptions as to the functional form of

[1] *Ap. J.*, **86**, 1, 1937.

[2] *M.N.*, **91**, 139, 1930; *ibid.*, p. 519, 1931.

[3] *Ibid.*, **89**, 620, 1929.

η_ν. The formulae assumed for η_ν contain in each case three parameters, and thus the results are applicable to a wide range of physical situations. With these solutions it is now possible to make a direct mathematical investigation of the effect on absorption lines of any simple monotonic variation of the absorption coefficients. We give these solutions here for reference as they are apparently not available elsewhere in the literature.

The equation of radiative transfer may be written, following Strömgren,

$$\frac{d^2J_\nu(t_\nu)}{dt_\nu^2} = \frac{3(1+\epsilon\eta_\nu)}{1+\eta_\nu}\left\{J_\nu(t_\nu) - \frac{1+\epsilon\eta_\nu Q}{1+\epsilon\eta_\nu}B_\nu(t_\nu)\right\}, \tag{1}$$

where t_ν, the optical depth in the line, is defined by

$$dt_\nu = (1+\eta_\nu)d\tau = -(1+\eta_\nu)\rho k_\nu dx\,. \tag{2}$$

We assume

$$\frac{1+\epsilon\eta_\nu Q}{1+\epsilon\eta_\nu}B_\nu(t_\nu) = a_\nu + p_\nu t_\nu\,,$$

and make the substitution

$$y(t_\nu) = J_\nu(t_\nu) - (a_\nu + p_\nu t_\nu)\,.$$

If we assume also that η_ν is a function of t_ν, the resulting differential equation for y may be solved in two general cases. We shall neglect $\epsilon\eta_\nu$ in (1), as when this is important $(1+\epsilon\eta_\nu)/(1+\eta_\nu)$ becomes simply ϵ, usually attributed to ionization cycles and hence roughly constant with t_ν. We then set, for the first solution (solution I),

$$1+\eta_\nu = A(1+D\tau)^s\,. \tag{3}$$

Substituting (3) in (2) and integrating for t_ν, (1) finally becomes

$$\frac{d^2y}{dt_\nu^2} = \frac{3}{A}(1+mt_\nu)^{-s/(s+1)}y\,, \tag{4}$$

where

$$m \equiv (s+1)\frac{D}{A}\,.$$

Equation (4) may be solved by the substitutions

$$z = 1 + mt_\nu ; \qquad w = \frac{2}{m}\sqrt{\frac{3}{A}}\,\gamma z^{1/2\gamma} ; \qquad \gamma \equiv \frac{s+1}{s+2},$$

provided s is not equal to -1 or -2, and we find

$$y = z^{1/2}\{c_1 I_\gamma(w) + c_2 K_\gamma(w)\},$$

where $I_\gamma(w)$ and $K_\gamma(w)$ are the usual Bessel functions of imaginary argument. Consideration of the boundary conditions $J_\nu = 2H_\nu$ at the surface and y equal 0 at infinity determines c_1 and c_2 and leads finally to the formula

$$r_\nu \equiv \frac{J_\nu(0)}{a_\nu} = \frac{1 + \left\{\frac{\sqrt{3A}}{2}\left(\frac{2p_\nu}{3a_\nu}\right) - \frac{\gamma}{\zeta}\right\}F_\gamma(\zeta)}{1 + \left\{\frac{\sqrt{3A}}{2} - \frac{\gamma}{\zeta}\right\}F_\gamma(\zeta)}, \tag{5}$$

where

$$\zeta \equiv \frac{2\sqrt{3A}}{(s+2)D}, \qquad \frac{\gamma}{\zeta} = \frac{(s+1)D}{2\sqrt{3A}}, \tag{6}$$

$$F_\gamma(\zeta) \equiv \begin{cases} -\dfrac{K_\gamma(\zeta)}{K'_\gamma(\zeta)} & \text{for} \quad D(s+2) > 0, \\ -\dfrac{I_\gamma(\zeta)}{I'_\gamma(\zeta)} & \text{for} \quad D(s+2) < 0. \end{cases}$$

In the simplified case that B_ν is given[4] by $a_\nu(1 + \frac{3}{2}\tau)$, $2p_\nu/3a_\nu$ is simply $d\tau/dt_\nu$, evaluated at an appropriate point. Taking this point to be $t_\nu = 1$, an "effective depth" of the line, we find

$$\frac{d\tau}{dt_\nu} = \frac{1}{A}\left(1 + \frac{(s+1)D}{A}\right)^{-s/(s+1)}. \tag{7}$$

[4] This is the case contemplated in the definition (5) of r_ν. For other situations we must replace a_ν by the intensity in the continuous spectrum just outside the line, and formulae (5), (8), (9), (12), and (13) became multiplied by the factor

$$\frac{1 + \frac{\sqrt{3}}{2}}{1 + \frac{\sqrt{3}}{2}\left(\frac{2b_\nu}{3a_\nu}\right)},$$

where b_ν is the continuous spectrum analogue of p_ν.

A consideration of the analysis as s approaches -1 and ∞ shows that (5) and (6) are valid in each limit. In the latter case $(s+1)D$ must approach some constant K and for (3) and (6) we have

$$1 + \eta_\nu = Ae^{K\tau}; \qquad \zeta = \frac{2\sqrt{3A}}{K}.$$

The former case corresponds to the one given by Eddington. The difference between his formula and (5) arises from his assumption that B_ν is linear in τ instead of, as here, in t_ν.

For s equal to -4, $-\frac{4}{3}$, $-\frac{8}{3}$, $-\frac{8}{5}$, $-\frac{12}{5}$, ... , etc., r_ν is expressible in terms of elementary functions, as γ becomes half-integral. For $D(s+2) > 0$ as well, $F_\gamma(\zeta)$ becomes a rational function of ζ; in the simplest case, $s = -\frac{4}{3}$, we find for positive D, using (7),

$$r_\nu = \frac{1 + \dfrac{9\left(1 - \dfrac{D}{3A}\right)^{-4}}{6\sqrt{3A} + 2D}}{1 + \dfrac{9A}{6\sqrt{3A} + 2D}} \approx \frac{1}{1 + \dfrac{9A}{6\sqrt{3A} + 2D}}, \tag{8}$$

the approximation holding provided D is less than A and A is large. Formula (8) corresponds closely to the physical situation represented by Eddington's solution ($s = -1$) and is considerably simpler to apply. For the limiting case $s = -2$, (5) no longer holds, but (4) becomes a homogeneous linear equation which can be solved directly, giving

$$r_\nu = \frac{\left(\dfrac{2p_\nu}{3a_\nu}\right) + \dfrac{D}{3A}\left(1 \pm \sqrt{1 + \dfrac{12A}{D^2}}\right)}{1 + \dfrac{D}{3A}\left(1 \pm \sqrt{1 + \dfrac{12A}{D^2}}\right)}, \tag{9}$$

where the plus sign goes with positive D and vice versa; $2p_\nu/3a_\nu$ may be expressed by (7) as before.

To determine A, D, and s in practical situations, we may use the values of η_ν and its derivatives with respect to τ, taken at some ap-

propriate point. Taking this point to be $\tau = 0$, and dropping the subscript ν, we find the formulae

$$\left.\begin{aligned} A &= 1 + \eta(0)\,, \\ s &= \frac{[\eta'(0)]^2}{[\eta'(0)]^2 - \eta''(0)[1 + \eta(0)]}\,, \\ D &= \frac{\eta'(0)}{s[1 + \eta(0)]}\,, \end{aligned}\right\} \tag{10}$$

where $\eta'(\tau)$ and $\eta''(\tau)$ stand for $d\eta_\nu/d\tau$ and $d^2\eta_\nu/d\tau^2$, respectively.

The second general solution (II) corresponds to the assumption

$$\frac{1}{1 + \eta_\nu} = L + Me^{-ut_\nu}\,. \tag{11}$$

Making the substitution

$$w = \frac{2}{u}\sqrt{3M}\; e^{-(u/2)t_\nu}\,,$$

we find

$$y = c_1 I_\delta(w) + c_2 K_\delta(w)\,,$$

where $\delta \equiv 2\sqrt{3L}/u$, and $I_\delta(w)$ and $K_\delta(w)$ are again Bessel functions of imaginary argument and of the first and second kinds, respectively. With boundary conditions as before, we find

$$r_\nu = \frac{1 + \left(\frac{2p_\nu}{3a_\nu}\right)\frac{1}{2}\sqrt{\frac{3}{M}}\, G_\delta\left(\delta\sqrt{\frac{M}{L}}\right)}{1 + \frac{1}{2}\sqrt{\frac{3}{M}}\, G_\delta\left(\delta\sqrt{\frac{M}{L}}\right)}\,, \tag{12}$$

where, for u positive,

$$G_\delta(w) \equiv \frac{I_\delta(w)}{I'_\delta(w)}\,.$$

For M negative both $\sqrt{M}$ and G_δ become imaginary, and in (12) we can take the absolute value of M and for G_δ the corresponding ratio of $J_\delta(w)$ and its derivative. In either case, when δ is equal to a

half-integer, $G_\delta(w)$ becomes expressible in terms of powers, and either trigonometric or hyperbolic functions of w.

Thus, for δ equal to $\frac{1}{2}$, we have for positive M

$$r_\nu = \frac{1 + \left(\frac{2p_\nu}{3a_\nu}\right)\frac{\sqrt{3}}{2\left(\sqrt{M}\coth\frac{1}{2}\sqrt{\frac{M}{L}} - \sqrt{L}\right)}}{1 + \frac{\sqrt{3}}{2\left(\sqrt{M}\coth\frac{1}{2}\sqrt{\frac{M}{L}} - \sqrt{L}\right)}}. \tag{13}$$

The $2p_\nu/3a_\nu$ factor, expressed in terms of L, M, and u by the method of (7), becomes simply $L + Me^{-u}$, and for $\eta_\nu(0)$ large the entire second term in the numerator may be neglected. For negative M we have merely to replace "coth" by "cot."

There is in this case no simple accurate expression for η_ν as an explicit function of τ. This is not important, however, since we proceed as in (10), determining L, M, and u from the derivatives of η_ν with respect to τ, evaluated at $\tau = 0$. As before we find

$$\left.\begin{aligned} u &= \frac{3[\eta'(0)]^2 - \eta''(0)[1 + \eta(0)]}{\eta'(0)[1 + \eta(0)]^2}, \\ M &= \frac{\eta'(0)}{u[1 + \eta(0)]^3}, \\ L &= \frac{1}{1 + \eta(0)} - M. \end{aligned}\right\} \tag{14}$$

In applying formulae (5) and (12) the physical meaning of assumptions (3) and (11), respectively, must be kept clearly in mind. A must, of course, be greater than 1 if $\eta_\nu(0)$ is to exceed zero; the values of D and s are not, however, so restricted. With assumption I for $1 + \eta_\nu$ we distinguish four particular cases.

1. $D>0$, $s>0$. η_ν increases with τ, and τ and t_ν go to infinity together. There are no singularities, and we may use (5) without hesitation. The condition on s gives, from (10), $\eta''(0) < [\eta'(0)]^2/[1 + \eta(0)]$.

2. $D<0$, $s<0$. Here η_ν increases with τ but becomes infinite for $\tau = -1/D$; beyond this point it becomes negative, or imaginary, etc., depending upon s. But if s is less than -1 (case 2*a*), t_ν becomes infinite at this point and thus η_ν

beyond becomes irrelevant and (5) is applicable. For $s > -1$ (case 2*b*) this is not true, and, in fact, the boundary conditions cannot even be satisfied. In 2*a* we have $\eta''(0) > 2[\eta'(0)]^2/[1 + \eta(0)]$.

3. $D>0$, $s<0$. η_ν decreases with τ. It approaches -1 eventually, but for D sufficiently small this is of no importance. For D large compared to A, however, the temperature gradient at $t_\nu = 1$ becomes very large, and we have an emission line; i.e., the negative absorption has been brought too near the surface. In general, this case must be used with suspicion, unless one is willing to fit solutions at $\tau = (A^{-1/s} - 1)/D$, as in Eddington's original paper. Note that for $s<-1$, t_ν remains finite as τ approaches infinity.

4. $D<0$, $s>0$. As in case 2 for $s>-1$, this case has nonphysical peculiarities and cannot be used, except in the limiting exponential case $s=\infty$, for which the singularity disappears and the boundary conditions may be satisfied. This suffers, however, from the same objection as case 3, since η_ν approaches -1 with increasing τ.

Thus, we see that (5) may be used with assurance only in cases 1 and 2*a* when η_ν is an increasing function of the optical depth. Similar cases may be drawn up for solution II and formula (12). Corresponding to the restriction $A > 1$ above, we have here the general condition $1 > L + M > 0$. It is clear that when u is negative, η_ν approaches -1, in one case decreasing monotonically and in the other becoming infinite for finite τ. The formula for $G_\delta(w)$ would be different here, but since this type of variation has already been discussed in connection with (5), and since it is of limited physical interest in any event, we shall not pursue it farther.

For positive u we note that if $\eta_\nu(\infty)$ is to be positive, L must lie between 0 and 1. Through (14) this together with the condition that u be positive imposes restrictions on $\eta''(0)$. For $\eta'(0)$ positive we find $\eta''(0) < 2[\eta'(0)]^2/[1 + \eta(0)]$; for $\eta'(0)$ negative, $\eta''(0) > [3 + 1/\eta(0)][\eta'(0)]^2/[1 + \eta(0)]$. When M is negative the condition of positive $M + L$ implies that the absolute value of M must be less than that of L. Thus the argument of $J_\delta(\delta\sqrt{M/L})$ is less than its order, and $J_\delta(w)$ is a monotonic function in the range considered.

We see that for $\eta'(0)$ negative we have a valid solution only for $\eta''(0)$ greater than the critical value given above. For $\eta'(0)$ positive, however, we have not only solution II but also I, cases 1 and 2*a*, as well, and can thus find r_ν for any values of $\eta''(0)$. For $\eta''(0) < [\eta'(0)]^2/[1 + \eta(0)]$ both formula (5) and formula (12) are equally valid. In general, both will presumably lead to very nearly the same result for

given $\eta(0)$, $\eta'(0)$, and $\eta''(0)$, but this conclusion is difficult to check. For γ and δ are given by different combinations of these quantities, and the only comparison possible is a purely numerical rather than an analytical one. In application, moreover, approximations must be made, since the Bessel functions are tabulated for only certain orders; either the values of the constants must be slightly changed to yield tabulated functions or interpolation must be resorted to. At the worst a good approximation may be had using (5) and (12) as two parameter formulae, taking $\eta(0)$ and $\eta'(0)$ as given, and adjusting $\eta''(0)$ to give the most easily calculated results. Applying this procedure to (13), for instance, we set $\delta=\frac{1}{2}$ or $u=4\sqrt{3L}$ in (14), and find a simple cubic equation for $\sqrt{L}$ in terms of $\eta(0)$ and $\eta'(0)$. For $\eta'(0)$ negative this has a single positive solution, but for $\eta'(0)$ positive there may be two such or even none. M is found directly from $\sqrt{L}$, $\eta(0)$, and $\eta'(0)$. The same method is easily extended to any value of δ.

PRINCETON, N.J.
September 10, 1937

UNIDENTIFIED INTERSTELLAR LINES IN THE YELLOW AND RED*

PAUL W. MERRILL AND O. C. WILSON

ABSTRACT

Six unidentified interstellar lines (Table 1) are discussed. Following a brief history of previous observations, Tables 2 and 3 give widths and central absorptions of three of the lines. The total intensity of λ 6284, which, in the mean, equals the average for the detached lines D1 and D2, shows a somewhat stronger correlation with stellar color excess than does the intensity of the D lines. The widths of the unidentified lines, which are rather diffuse and not sharp like the D lines, and other facts make an atomic origin improbable. The lines may be portions of molecular bands, as yet unidentified. Several facts, however, suggest that the lines are produced by small solid particles, perhaps closely related to those that cause space reddening.

INTRODUCTION

In 1920, Miss Mary L. Heger at Lick Observatory measured two faint absorption lines, λ 5780 and λ 5797, in several B-type spectra, notably that of ζ Persei.[1] She evidently recognized the possibility that they might be "stationary" but considered the data inconclusive. About the same time W. H. Wright recorded a weak line at λ 6283 in the spectrum of α Cygni[2] but marked it "probably of atmospheric origin."

More recently the lines λλ 5780, 5797, 6284, and 6614 were observed at Mount Wilson, in the spectrum of HD 183143,[3] but, on account of their lack of sharpness, their interstellar origin was not immediately recognized. Their occurrence in numerous spectra of types Oa–A4 later roused suspicion, however, and correlations of their intensities with distance[4] and color excess were then soon noted.

The nonstellar origin of λ 5780 and λ 6284 was definitely shown by their failure to participate in the periodic displacements of lines of

* *Contributions from the Mount Wilson Observatory, Carnegie Institution of Washington*, No. 582.

[1] *Lick Obs. Bull.*, **10**, 146, 1921.

[2] *Ibid.*, p. 109.

[3] *Mt. W. Contr.*, No. 409; *Ap. J.*, **72**, 98, 1930. [4] *Pub. A.S.P.*, **46**, 206, 1934.

the spectroscopic binary Boss 6142[5] and by the fact that the observed wave lengths appear, in general, to be independent of the motions of the stars in whose spectra the lines occur.[6]

WAVE LENGTHS

Although the positions of these lines have been measured on many spectrograms, the accuracy of the mean wave lengths is still not very high. On half the plates the lines are near the limit of visibility, and, even with spectrograms of good quality where the lines are fairly intense, the probable error of a single plate (two independent measures) is about 0.2 A, the slightly diffuse character of the lines preventing greater precision. Except for the high contrast and fine grain of the III C emulsion,[7] with which most of the negatives were made, the accuracy would have been still lower. The wave lengths computed on the assumption that the displacements are the same as those of the D lines in the same spectra are in Table 1.

TABLE 1

WAVE LENGTHS OF INTERSTELLAR LINES

λ	Intensity	No. Plates
5780.55 ± 0.03	3	229
5797.13 ± .04	1	141
6202.99 ± .06	1—	9
6269.99 ± .04	1	14
6283.91 ± .03	6	219
6613.9 ± 0.1	2	39

The lines λ 6203 and λ 6270, which were not included in the original investigation, occur on spectrograms on which λ 6284 is strong. Reduction of the measures on the assumption that the lines are of stellar origin gives the wave lengths 6202.98 ± 0.12 and 6270.10 ± 0.08. Since the probable errors obtained by using velocities derived from the interstellar D lines (see Table 1) are only half these values, the evidence for interstellar origin is strong.

[5] *Mt. W. Contr.*, No. 536; *Ap. J.*, **83**, 126, 1936.

[6] *Pub. A.S.P.*, **48**, 179, 1936.

[7] Supplied by the Eastman Kodak Co.

LINE STRUCTURE

The interstellar D lines, like H and K, are extremely sharp and well defined, their apparent shapes undoubtedly being determined largely by the limitations of the spectrograph and of the photographic plate. The unidentified lines under discussion are, however, quite different in character, being wider and softer, with diffuse edges. They resemble stellar lines of intermediate sharpness, which,

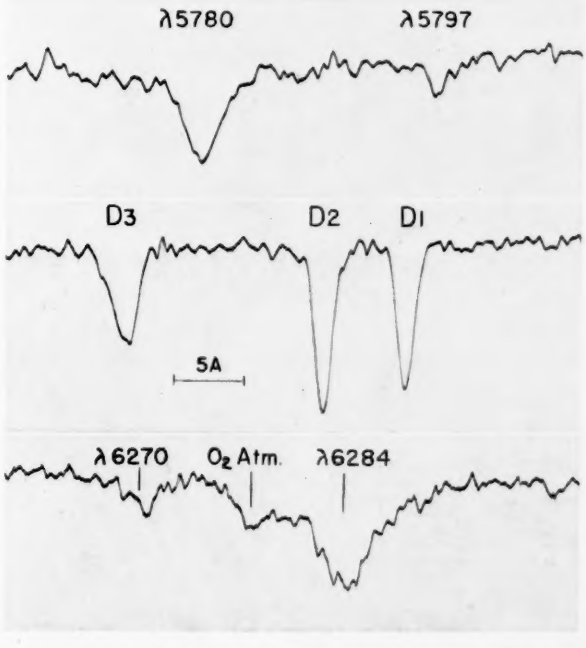

FIG. 1.—Tracings of interstellar lines in the spectrum of HD 183143

although not extremely broad and hazy, might be described as "somewhat diffuse" or "not sharply defined" (see Fig. 1; see also Pl. X and Fig. 2 of *Mt. W. Contr.*, No. 576).[8]

The actual widths of the lines, as well as the total absorptions or equivalent widths, were determined from photometric tracings (scale, 100 times original, or 0.336 A/mm) of a large number of photographs by noting the points at which the line profiles begin to drop

[8] *Ap. J.*, **86**, 274, 1937.

below the level of the adjacent continuous spectrum. Although line edges cannot be located with precision on individual spectrograms, the observations are sufficiently numerous to yield good mean val-

TABLE 2

MEASURED WIDTH IN ANGSTROMS

EW	λ 5780	λ 5797	λ 6284	$D_{2,1}$
0.05 A	.....	(2.7)	.....	(1.5)
0.1	4.0	3.2	.....	1.7
0.2	4.6	(3.8)	6.9	2.2
0.4	6.2	.....	7.9	2.7
0.6	7.4	.....	9.1	3.1
0.8	(8.0)	.....	10.1	3.4
1.0	.....	.....	11.4	3.7

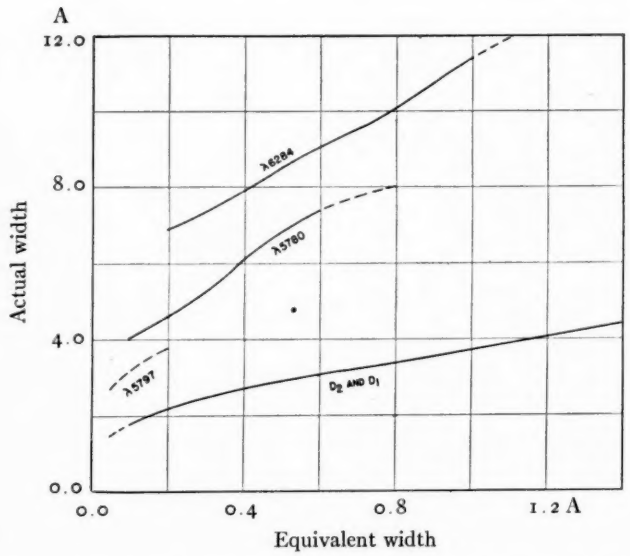

FIG. 2.—Actual width and equivalent width. The dispersion of the original spectrograms is 33.6 A/mm.

ues. To secure homogeneity all the photometric measurements were made by the same observer (O. C. W.).

The results are shown in Table 2 and in Figure 2. For a given equivalent width, λ 6284 is wider than λ 5780, while λ 5797 is prob-

ably narrower. The measured widths of the D lines, included for comparison, depend to a large degree upon the purity of the spectrum and the properties of the photographic plate, as well as on the intrinsic line widths.

TABLE 3

CENTRAL ABSORPTION IN PERCENTAGE

EW	λ 5780	λ 5797	λ 6284	D2, 1	*Si* II
0.5	.....	3	.....	5	3
0.1	5	6	4	9	5
0.2	8	11	6	17	12
0.4	14	.....	10	30	23
0.6	19	.....	14	41	33
0.8	(25)	.....	18	50	40
1.0	.....	.....	20	58	(45)
1.2	.....	.....	23	65	.....

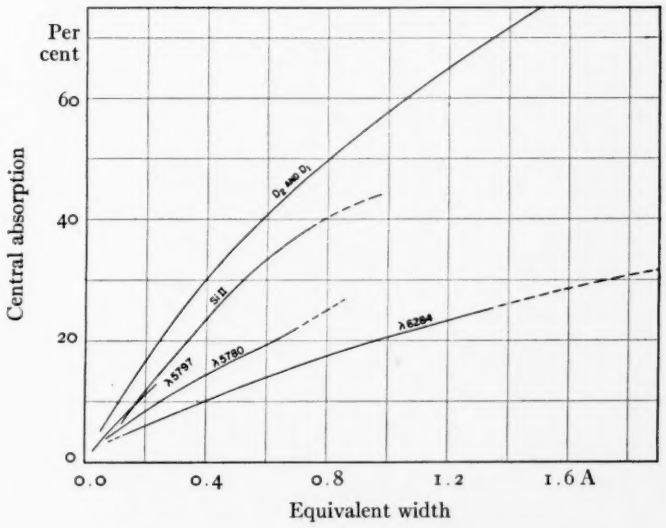

FIG. 3.—Central absorption and equivalent width

A similar comparison of the measured central absorptions appears in Table 3 and in Figure 3. The values for the D lines are undoubtedly too small because of limitations imposed by the spectrograph and the photographic emulsion. The values for the other lines, however, should be reasonable approximations to the intrinsic central ab-

sorptions.[9] Since the number of images measured is considerable and the scatter of individual values is not large, the means, and especially their relative values, should be reliable. For a given equivalent width, λ 6284 is shallower than λ 5780, and λ 5797 is deeper, while all three lines are markedly shallower than the D lines. These results are in harmony with those found from the actual widths.[10] The stellar *Si* II lines,[11] λ 6347 and λ 6371, included in Table 3 for comparison, are decidedly deeper than λ 5780 and λ 6284. The structure of λ 5797, on the other hand, as far as indicated by the meager data, does not differ radically from that of the silicon lines. Little can be said concerning the structure of λ 6203 and λ 6270; they are perhaps slightly more diffuse than λ 5797.

The lack of identical structure in λλ 5780, 5797, and 6284 indicates that, if these lines belong to an atomic multiplet, it is one with quite unusual properties.

Concerning the symmetry of the lines no very definite statement can be made. λ 5780 usually appears symmetrical, although in about ten instances an apparent asymmetry is noticeable on the tracings, and in all but one of these the violet edge is steeper, suggesting that possibly a faint companion lies toward the red from the main component. We are inclined to think, however, that as a first approximation the line is to be regarded as symmetrical. λ 5797 is too weak and narrow to give a positive result and λ 6284 is too involved with near-by lines of the alpha band of terrestrial oxygen.

TOTAL INTENSITY

The integrated intensities of the lines λλ 5780, 5797, and 6284, expressed in equivalent widths or angstroms of complete absorption, are recorded for individual stars in *Mt. W. Contr.*, No. 576.[8] A graphical comparison in Figure 4 shows that throughout the observed range the intensity of λ 5780 is, on the average, very nearly one-half that of λ 6284 and slightly more than three times that of

[9] Unless, of course, the lines are formed by several narrow, unresolved components.

[10] The agreement is not a mathematical necessity because a line with a narrow core might conceivably be both wider and deeper than another one of the same equivalent width.

[11] Largely from spectra of c stars.

λ 5797. The intensity of λ 6614, for which only one or two measurements are available, appears to be between that of λ 5780 and of λ 5797. The scatter of the relative intensities, although considerable, does not certainly exceed errors of measurement, which, because of lack of sharpness in the lines, are considerable. The intensity of λ 5797 is below that required for the best determinations,

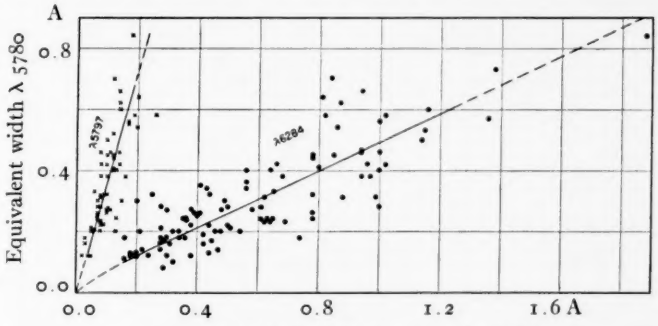

FIG. 4.—Comparison of equivalent widths of λ 5780, λ 5797, and λ 6284

TABLE 4

TOTAL INTENSITIES OF λ 5797 AND λ 6270

STAR	HD	EA	
		λ 5797	λ 6270
	4841	0.16	0.15
	14818	.....	.09
χ² Ori	41117	.08	.09
	20041	.14	.11
	183143	.18	.33
Boss 6111.....	223385	0.12	0.10

while measurements of λ 6284 are made difficult by the presence, in the violet wing, of lines belonging to the head of the alpha band of terrestrial oxygen.

According to eye estimates, the intensity of λ 6270 is nearly equal to that of λ 5797, while that of λ 6203 is somewhat less. Total intensities measured from photometric tracings of a few spectra are in Table 4.

In the spectrum of HD 183143 (see Fig. 1) the intensity of λ 5797 appears unusually low relative to that of the other unidentified detached lines.

Since the intensities of λ 5780 and λ 6284 are closely correlated, a combination value has been used in the following discussions. A smooth curve, drawn through the plot (Fig. 4) representing ob-

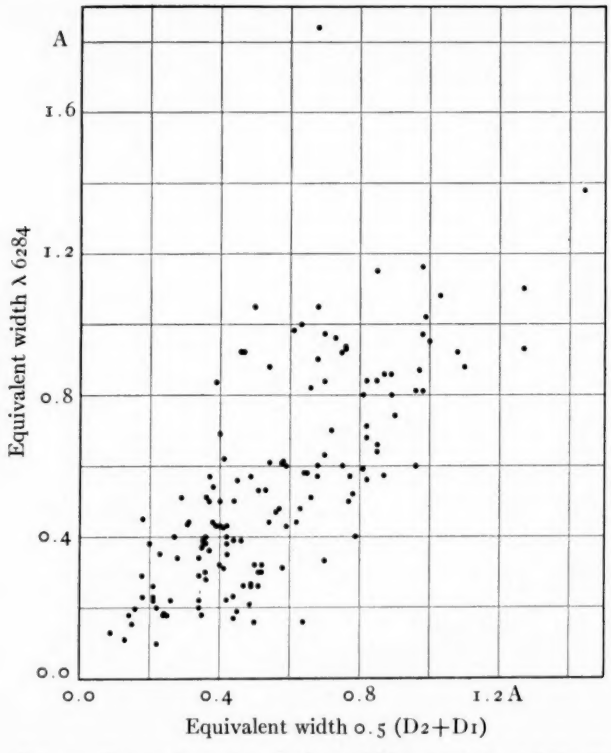

FIG. 5.—Comparison of equivalent widths of λ 6284 and the D lines

served pairs of values, was used to obtain from each measurement of λ 5780 a hypothetical intensity of λ 6284 which was combined (weight one-half) with the measured intensity. The result is denoted by I' λ 6284.

Upon plotting the equivalent width I'λ 6284 against that of the D lines, 0.5 (D2 + D1), called $I'D$ (Fig. 5), a strong correlation appears, although the scatter is obviously greater than that caused by error of measurement. The relatively great intensity of λ 6284,

equal in the mean to that of the average of the two D lines, may cause surprise. It would perhaps not be anticipated from visual inspection of the negatives, for the eye often underestimates the total intensity of a broad, shallow line compared with a narrow, deep one. The correlation coefficient for $I'D$ and $I'\lambda$ 6284, from 127 stars, is $+0.71 \pm 0.03$.

A statistical dependence of the intensity of λ 6284 upon stellar distance (length of light-path), to be expected from the facts now

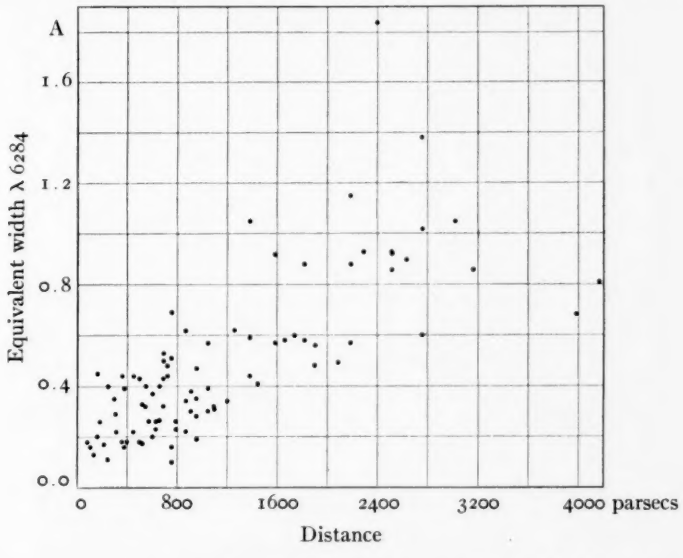

FIG. 6.—Stellar distance and intensity of λ 6284

available, is shown by Figure 6. The observed irregularities are not markedly greater than those exhibited by the calcium[12] or sodium[13] lines, although the measurements are probably less accurate. For all the lines the scatter at the greater distances and among the more intense lines is large. Because of the relatively small central absorption, the equivalent widths of λ 6284 in various spectra should be nearly in direct proportion to the total numbers of absorbing particles encountered by the light-beam.[14] The scatter in the distance-

[12] *Mt. W. Contr.*, No. 573; *Ap. J.*, **86**, 136, 1937.

[13] *Mt. W. Contr.*, No. 569; *Ap. J.*, **86**, 28, 1937.

[14] Provided the line is not formed by narrow, unresolved components.

intensity relationship would thus measure differences in the average concentration of particles in different directions. With the narrow calcium or sodium lines, on the other hand, variations in velocity along the light-path play an important role, and the relationship becomes more complicated.

LINE INTENSITY AND COLOR EXCESS

Because interstellar line intensity and space reddening both increase with distance, they should exhibit a positive correlation with

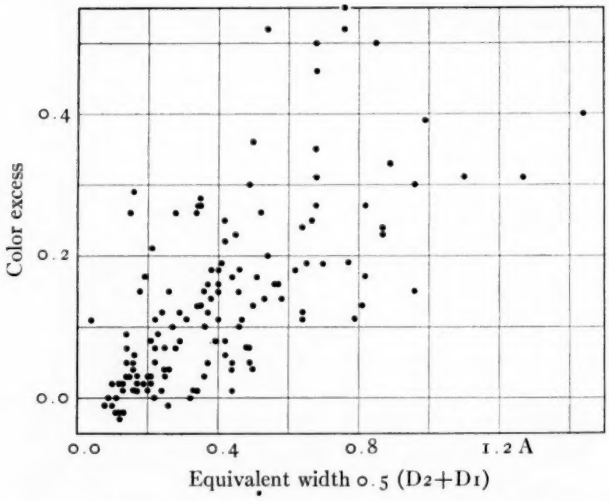

FIG. 7.—Color excess and intensity of the D lines

each other. This expectation has been verified for the K line by E. G. Williams[15] and by R. F. Sanford.[16]

Eighty-five stars with observed intensities of λ 6284 and the D lines have colors measured by Stebbins and Huffer[17] or by W. Becker.[18] Scatter diagrams for color excess against $I'D$ and against $I'\lambda$ 6284 are shown in Figures 7 and 8, respectively, in both of which a positive correlation is obvious.

[15] *Mt. W. Contr.*, No. 487; *Ap. J.*, **79**, 280, 1934.

[16] *Mt. W. Contr.*, No. 573; *Ap. J.*, **86**, 136, 1937.

[17] *Pub. Washburn Obs.*, **15**, 217, 1934. Messrs. Stebbins and Huffer have kindly sent us additional unpublished data.

[18] *Veröffentlichungen der Universitätssternwarte zu Berlin-Babelsberg*, **10**, 1, 1933.

Because the identification of λ 6284 is as yet uncertain, it is important to follow all clues which may bear on the origin of the line. Thus it is desirable to determine whether the intensity of λ 6284 or that of the D lines is more closely correlated with color excess (space reddening). The appearance of Figures 7 and 8 favors a higher correlation for λ 6284—a conclusion borne out by the correlation co-

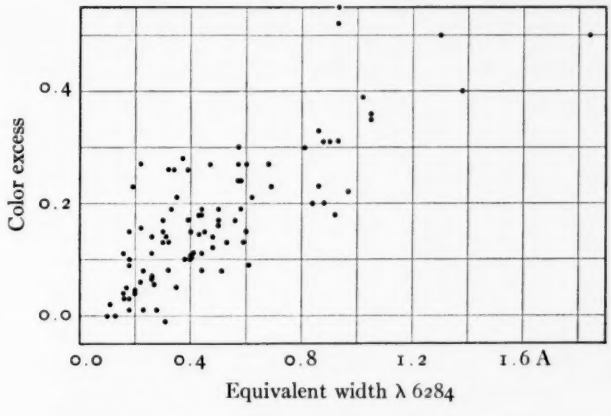

FIG. 8.—Color excess and intensity of λ 6284

efficients given in Table 5, which have been computed from the standard formula,

$$r = \frac{\Sigma xy}{N\sigma_1\sigma_2}.$$

For the 85 stars with complete data the coefficient for color excess and I' λ 6284 is +0.81 ± 0.03, while that for color excess and $I'D$ is only +0.61 ± 0.05. Similar results are found when the 85 stars are divided into two groups with $I'D < 0.50$ A, and between 0.50 and 1.44 A; and again for 17 O-type stars. These computations with a few others for comparison are summarized in Table 5.

What is the proper interpretation of these results, which, taken at face value, indicate that λ 6284 has a closer connection with space reddening than the D lines? Is a physical relationship between space reddening and intensity of λ 6284 to be inferred? Since the D lines arise from absorption by gaseous sodium atoms, while space reddening is probably caused by finely divided dust, a close physical de-

pendence in this instance is unlikely. Were both sodium gas and the dust uniformly distributed through space, a very high correlation of $I'D$ and color excess would nevertheless be expected. The moderate values of the coefficients recorded in Table 5 indicate considerable irregularities in distribution. May we conclude from the stronger correlation between color and $I'\lambda\,6284$ that the source of this line is in some way connected with the dust particles? Errors of measurement are larger for $\lambda\,6284$ than for the D lines and would therefore tend to weaken the correlation relative to that of the D lines rather than to strengthen it. On the other hand, the approach to saturation may give more scatter to the values of $I'D$, the effect being

TABLE 5*

CORRELATION COEFFICIENTS

Objects		No.	E, $I'D$	E, $I'\lambda\,6284$	$I'D$, $I'\lambda\,6284$
Stars having complete data	All	85	+0.61±0.05	+0.81±0.03	+0.68±0.04
	Weak D	45	.40± .08	.54± .07	.46± .08
	Strong D	40	.41± .09	.81± .04	.46± .08
Stars having E and $I'D$		139	.73± .03	.....	.....
O types		17	+0.44±0.13	+0.61±0.10	+0.39±0.14

*E = Color excess (Stebbins and Huffer, and Becker); $I'D$ = intensity $0.5(D_2 + D_1)$; $I'\lambda\,6284$ = "smoothed" intensity of $\lambda\,6284$.

negligible for $\lambda\,6284$. Even for the D lines, however, the effect cannot be very great, unless possibly for extremely intense lines, because intensity is, on the average, nearly proportional to distance.[19]

ORIGIN OF THE LINES

Because of the very long intervals between collisions resulting from the low density, particles in interstellar space capable of emitting light must spend practically all their time in the quantum level of least energy. Even levels ordinarily called "metastable" probably do not persist long enough to cause any important exceptions to this rule. Interstellar absorption lines should therefore be resonance lines. Atomic lines of this kind, with the possible exception of those belonging to very rare atoms, should be well known in the laboratory. The difficulty of identification of the new interstellar

[19] The mean distance-intensity relationship is $I'D = c \times (\text{Distance})^{0.86}$. See *Mt. W. Contr.*, No. 569; *Ap. J.*, **86**, 28, 1937.

lines in the visual region may thus be taken as an argument against an atomic origin.

The width of the lines, moreover, seems incompatible with an atomic origin. Since the lower level of an interstellar absorption line must have an extremely long life, the line would be very sharp. The upper level might conceivably be one of very short life, perhaps with energy in excess of ionization, but this situation seems improbable as it would call for a lower level of high energy with incredibly great metastability.

An approximation to a (hypothetical) damping constant for the line λ 6284 may be obtained as follows. Since the line is relatively shallow even for a considerable total intensity, the equivalent width in angstroms may be written

$$W = 10^8 \frac{\pi e^2 \lambda^2}{mc^2} Nf .$$

For an equivalent width of 1 A, this equation gives $Nf = 2.9 \times 10^{12}$. The optical thickness is

$$\tau = Nf\sigma ,$$

where σ, the atomic absorption coefficient, may be written

$$\sigma = \frac{\delta}{(\nu - \nu_0)^2 + \delta^2} \times \frac{e^2}{mc} ,$$

δ being the quantum-mechanical analogue of the classical damping constant. At the center of the line

$$\tau_0 = \frac{Nfe^2}{mc\,\delta} .$$

Table 3 shows that for an equivalent width of 1 A, λ 6284 has a central absorption of 20 per cent. On account of the width of the line, this value is probably not seriously affected by photographic effects or by the finite purity of the spectrum. Hence we may write

$$1 - e^{-\tau_0} = 0.20 ,$$

from which

$$\tau_0 = 0.22 = \frac{2.42 \times 10^{10}}{\delta} .$$

Hence $\delta = 1.1 \times 10^{11}$, which is about two thousand times the value of the classical damping constant

$$\gamma = \frac{8\pi^2 e^2 \nu^2}{3mc^3} = 5.7 \times 10^7 \text{ (for } \lambda\, 6284) .$$

If λ 6284 is produced by an atom whose thermal motions are responsible for the width, the atomic mass must be very small. If the optical thickness at the center of the line is 0.22, that at distance $\Delta\lambda$ from the center may be taken to be

$$\tau_{\Delta\lambda} = 0.22 e^{-(\Delta\lambda/b)^2} .$$

Our measurements show that, for an absorption of 5 per cent, $\Delta\lambda = 3.4$ A. Hence $b = 2.8$ A. Since

$$b = \frac{\lambda_0}{c}\sqrt{\frac{2KT}{m}} ,$$

it follows that

$$m = 1.5 \times 10^{-30} \times T .$$

For the lightest atom known, that of hydrogen, $T = 1{,}100{,}000°$, an inadmissibly high value, while for heavier atoms T is still greater. For $T = 40{,}000°$, which is probably an upper limit,[20] $m = 6 \times 10^{-26}$, which is only one-thirtieth the mass of the hydrogen atom, while for $T = 10{,}000°$ it is 1.5×10^{-26}, or only about twenty times the mass of the electron. These considerations make it very improbable that λ 6284 is an atomic line broadened by Doppler effect.

A second hypothesis is that the lines are actually bands or portions of bands of molecular origin. Under the prevailing excitation, molecules would be concentrated in a few of the lower quantum levels, and the band structure might thus differ from that observed in the laboratory. The low density of interstellar space favors both ionization and dissociation, but since neutral atoms (of sodium) are known to be fairly abundant, one can scarcely decide a priori against the existence of molecules. Among the writers who favor the molecular hypothesis, two have made specific suggestions. P. Swings[21] has called attention to the fact that λ 6613.9 and λ 6283.91 fall approximately in the calculated positions of bands of carbon dioxide. The second coincidence is not very close ($\Delta\lambda = 3.0$ A), but

[20] *Mt. W. Contr.*, No. 570; *Ap. J.*, **86**, 44, 1937. [21] *M.N.*, **97**, 212, 1937.

Swings thinks it may be within the uncertainties of measurement and calculation. A spectrogram of χ^2 Orionis taken by Dr. Theodore Dunham, Jr.,[22] which includes the region of the "Venus" bands at λ 7820 and λ 7883 and fails to show definite absorption at or near these wave lengths, gives a negative answer to the test suggested by Swings.

M. N. Saha[23] has recently suggested that λ 6284 "appears decidedly to be due to molecular sodium, Na_2, due to the transition (Na_2: $^2S^2S\,A'\Sigma - {}^2S^2P\,B'\Sigma$, $n'' = 0, n' = 8$)" and that λ 5780 "may be provisionally identified with a line of NaK ($n'' = 0$, $n' = 5$)." Detailed calculations of the structure of these bands and of the relative intensities of neighboring related bands will probably be required before the identifications can be conclusively established.

A third possibility is that the unidentified lines are produced by small solid particles. This hypothesis is suggested by the fact that the correlation between color excess and the intensity of λ 6284 seems to point toward a physical relationship between space reddening and the formation of the spectral line. At room temperature only a few solids are known to produce narrow absorption lines, but at very low temperatures many, although not all, substances probably have narrow lines which may be thought of as displaced atomic lines.[24] It is therefore conceivable that at temperatures a few degrees above absolute zero, the interstellar dust which causes the reddening of star light might also produce certain detached lines. This surmise, if correct, offers the future possibility of a partial chemical analysis of dark nebulae. A theoretical investigation of the formation of absorption lines by solids in the form of finely divided dust would be valuable, while data on lines produced in the laboratory by solids at low temperatures should be examined for possible coincidences in wave length.

An alternative interpretation of the data might be that the lines have their origin in a gas which is in some way dependent on the dust particles and thus tends to occupy the same regions of space.

CARNEGIE INSTITUTION OF WASHINGTON
MOUNT WILSON OBSERVATORY
August 1937

[22] Who kindly permits reference to it here. [23] *Nature*, **139**, 840, 1937.
[24] See, e.g., Spedding and Nutting, *J. Chem. Physics*, **2**, 421, 1934.

RELATIVE *f*-VALUES FOR LINES OF *Fe* I AND *Ti* I*

ROBERT B. KING AND ARTHUR S. KING

ABSTRACT

The relative *f*-values for 115 lines in 19 multiplets of *Fe* I between λ 2912 and λ 5455 and for 227 lines in 66 multiplets of *Ti* I between λ 3123 and λ 6743 have been derived from measurements on electric-furnace absorption spectrograms. The method is essentially the same as that described in *Mt. Wilson Contr.*, No. 528, which gave results for 75 lines in 9 multiplets of *Fe* I.

All the lines arise from the lowest terms in the atoms, ranging in excitation potential from 0.0 to 1.5 volts for *Fe* I and from 0.0 to 2.5 volts for *Ti* I.

The relative *f*-values of lines in multiplets of *Fe* I and *Ti* I have been measured with the electric furnace as the source of the absorption-spectrum excitation. The method used has been described in detail in an earlier paper on relative *f*-values for lines of *Fe* I.[1] This paper will be referred to in the following as "(1)." The method will be summarized briefly here, and modifications made in the present work will be pointed out.

The elements have been vaporized in the furnace at known temperatures, and their spectra observed in absorption. The relative total absorptions of the lines appearing on the linear (faint-line) portion of the curve of growth were measured and, with the aid of this curve, converted into relative intensities for the given temperature. The relative *f*-values are then obtained by the application of Boltzmann factors to the observed relative intensities of lines arising from different energy-levels. Boltzmann factors may be applied because of the existence of a close approximation to thermal equilibrium at a known temperature in the furnace. This condition was tested in (1) and found to hold within the limits of experimental error.

OBSERVATIONS AND PHOTOMETRY

The absorption spectrum to be studied was obtained by passing the light from a 50-amp. Philips cinema lamp with quartz bulb

* *Contributions from the Mount Wilson Observatory, Carnegie Institution of Washington*, No. 581.

[1] R. B. King and A. S. King, *Mt. W. Contr.*, No. 528; *Ap. J.*, **82**, 377, 1935.

through the furnace tube and to the slit of the 15-foot concave-grating spectrograph. The newer hood furnace was used in place of the cylindrical furnace employed in the earlier work because a constant temperature was more readily maintained.

The spectrum to the violet of about λ 5400 was, as a rule, photographed in the second order, while the first order was used to the red of this limit. Eastman IV-O and IV-F plates were used, the fine-grained, high-contrast emulsion being most satisfactory for the photometry of faint absorption lines.

In the previous work all the exposures were made at a furnace temperature of 2100° C, the intensities of the lines being altered for different exposures by varying the charge of material in the furnace. This alteration of intensity is necessary in order that a large intensity range may be treated, the linear portion of the curve of growth covering only a short range. The change in the strength of the lines can, however, be more readily controlled by changing the temperature, as well as the charge of material, in the furnace for different exposures; in the present work, temperatures ranging from 1800° C to 2600° C were used. The low temperatures bring the strongest lines to the linear portion of the curve of growth, and the high temperatures the fainter lines. Practically all the *Fe* and *Ti* lines of temperature classes I and II and many of class III were thus brought onto the straight portion of the curve.

Temperature measurements were made on the inner walls of the furnace tube by means of an optical pyrometer, checked for accuracy by means of a tungsten ribbon lamp calibrated by the Bureau of Standards. Correction was made for absorption by the furnace window. The uncertainty in the temperature readings was usually less than 20° C. The actual uncertainty, of course, also depends upon the uncertainty of the temperature scale at these temperatures.

Calibration marks were impressed on the plates by means of a ribbon-filament lamp and a step-slit, as described in (1). Plates were developed in X-ray developer at 18° C, as before.

Tracings of both furnace and calibration spectra were made with the photoelectric microphotometer designed by Dunham. The high resolving-power and sensitivity of this instrument are well suited to photometry of faint absorption lines.

REDUCTION OF OBSERVATIONS

Characteristic curves constructed for each plate at wave-length intervals of about 100 A were used to derive the equivalent widths of the absorption lines in angstrom units. In the work reported in (1), the areas under the density contours of the lines were converted into intensity areas, which were then measured. For the present work a shorter method has been adopted. It happens that the Doppler width of lines of *Fe* and *Ti* at the upper limit of the linear portion of the curve of growth for the temperatures used is less than the width of the slit image formed on the plate even in the second order. That is, with a slit-width of 0.015 mm the faint lines falling on the linear portion of the curve of growth appear on the microphotometer tracings as small triangles with the same base-width. The altitudes of the triangles are therefore proportional to the equivalent widths of the lines. The base-width varies directly with the wave length and, in angstrom units, is very nearly twice as large in the first order as in the second, owing to the increased resolving-power of the second order. Mean values of the base-width as a function of the wave length were determined for the first and second orders and used together with the measured altitudes of the triangular contours to obtain equivalent widths.

The approximate linearity under our experimental conditions of the "straight" portion of the curve of growth for faint lines was verified in (1). In the present work an empirical curve of growth was used to reduce the equivalent widths to relative intensities. This curve was constructed by plotting the equivalent widths, obtained by treating the line contours as triangles, against Harrison's[2] arc-intensity measurements for several multiplets of *Ti* I as described in (1). The resulting curve differed only very slightly from the theoretical linearity.

The total absorption A_T of a line formed by passing a continuous spectrum through an absorbing column of gas has been defined[3] as the ratio of the energy absorbed by the line to the incident energy:

$$A_T = \frac{I}{I_0}.$$

[2] G. R. Harrison, *J. Opt. Soc. Amer.*, **17**, 389, 1928.

[3] R. Ladenburg and F. Reiche, *Ann. d. Phys.*, **42**, 181, 1913.

On the linear portion of the curve of growth the total absorption A_T in a frequency interval $d\nu$ is directly proportional to the number of atoms absorbing the line:

$$A_T d\nu \propto Nf,$$

where N is the number of atoms in the lower energy-level involved in the transition and f is the f-value, or "oscillator strength" of the line. Then

$$\frac{A_T d\lambda}{\lambda^2} \propto Nf.$$

Hence, if $d\lambda$ is measured in angstrom units, the quantity $A_T\, d\lambda$ is the equivalent width EW, the fraction of an angstrom unit of the neighboring continuous spectrum totally absorbed by the line. So we can write

$$\frac{EW}{\lambda^2} \propto Nf.$$

We are concerned here only with the relative numbers of atoms in the various low levels. These depend upon the temperature of the gas, the distance of the levels above the normal state, and the statistical weights, g, of the levels. If the gas is in thermal equilibrium, a Boltzmann factor may be used to allow for the temperature distribution of the atoms among the low energy-levels. Hence,

$$N \propto e^{-\frac{hc}{KT}\Delta\nu} g,$$

where $\Delta\nu$ is the wave-number difference between the low level from which the absorption line arises and the lowest energy-level in the atom, and T is the absolute temperature. We have then

$$\frac{EW}{\lambda^2} \propto e^{-\frac{hc}{KT}\Delta\nu} gf$$

and

$$f \propto \frac{EW}{\lambda^2} \frac{e^{\frac{hc}{KT}\Delta\nu}}{g}.$$

The procedure followed was to derive from the linear portion of the empirical curve of growth numbers corresponding to the relative intensities of the lines on each spectrogram. Then, since a variety of temperatures was used, Boltzmann factors were applied. Intensities from different spectrograms were reduced to the same scale by means of factors obtained from lines appearing on two or more spectrograms, and all the data for each line averaged to obtain the adopted mean values.[4] These intensity numbers, when divided by λ^2, are relative *gf*-values. It has been pointed out that to correspond to true relative *f*-values these must be divided by the statistical weight, $g = (2j + 1)$, of the lower level involved in the transition.[5] Since this was not done in (1), the values there published are really *gf*-values. Since relative *gf*-values are also convenient for astrophysical applications, they, as well as the relative *f*-values, are listed in the tables of results.

RESULTS

Fe I.—Relative *gf*- and *f*-values, the former on an arbitrary scale, for 115 lines in 19 multiplets of *Fe* I between λ 2912 and λ 5455 are given in Table 1. For completeness the results for the 75 lines in 9 multiplets between λ 3649 and λ 4325 published in (1) are also included in the table. The number of spectrograms used in the means (last column of table) indicates roughly the weight of the results. Values which are particularly uncertain because the lines were very faint on the spectrograms are marked with an asterisk. A few of the strongest lines whose measures were regarded as uncertain are also thus indicated.

All lines measured arise from the a^5D, a^5F, and a^3F levels, the three lowest even levels in *Fe* I, whose excitation potentials are 0.0, 1.0, and 1.5 volts, respectively. Only lines arising from these three low terms are observed in absorption at the temperatures used.

Of the 29 multiplets listed, only 7 are completed. In most cases the fainter members were not observed. For multiplets Nos. 172 and 203, however, the strongest lines were too strong to appear on the

[4] The method followed in (1) differed from this procedure in that, since all measures were made at a single temperature (2100° C), a single set of Boltzmann factors for this temperature was applied after the measures were reduced to the same scale.

[5] D. H. Menzel and L. Goldberg, *Ap. J.*, **85**, 40, 1937.

TABLE 1

RELATIVE *gf*- AND *f*-VALUES FOR LINES OF *Fe* I

Mult. No.	λ	Multiplet	*gf*	*f*	No. of Plates
78.....	2912.16	$a^5D_4-y^5F^\circ_5$	10	1.1	2
	2929.01	$a^5D_3-y^5F^\circ_2$	13.5	1.9	2
	2936.90	$a^5D_4-y^5F^\circ_4$	25	2.8	6
	2941.35	$a^5D_2-y^5F^\circ_1$	12	2.3	1
	2947.88	$a^5D_3-y^5F^\circ_3$	28	4.0	6
	2953.94	$a^5D_2-y^5F^\circ_2$	28	5.6	6
	2957.37	$a^5D_1-y^5F^\circ_1$	22	7.4	6
	2965.26	$a^5D_0-y^5F^\circ_1$	17	17	5
	2966.90	$a^5D_4-y^5F^\circ_5$	43	4.7	7
	2970.10	$a^5D_1-y^5F^\circ_2$	27	9.0	6
81.....	2981.45	$a^5D_3-z^3P^\circ_2$	14	2.0	8
	2986.46	$a^5D_1-z^3P^\circ_1$	3.5	1.2	5
	3007.29	$a^5D_2-z^3P^\circ_2$	11	2.2	6
	3024.04	$a^5D_1-z^3P^\circ_2$	16	5.2	8
84.....	2983.57	$a^5D_4-y^5D^\circ_3$	36	4.0	6
	2994.44	$a^5D_3-y^5D^\circ_2$	43	6.1	7
	3001.00	$a^5D_2-y^5D^\circ_1$	46	9.2	6
	3008.14	$a^5D_1-y^5D^\circ_0$	35	12	6
	3017.63	$a^5D_1-y^5D^\circ_1$	16	5.2	6
	3020.49	$a^5D_2-y^5D^\circ_2$	29	5.8	6
	3020.64	$a^5D_4-y^5D^\circ_4$	51	5.7	5
	3021.07	$a^5D_3-y^5D^\circ_3$	63	9.0	6
	3025.85	$a^5D_0-y^5D^\circ_1$	34	34	6
	3037.39	$a^5D_1-y^5D^\circ_2$	45	15	6
	3047.61	$a^5D_2-y^5D^\circ_3$	45	9.0	7
	3059.09	$a^5D_3-y^5D^\circ_4$	38	5.4	7
85.....	2987.30	$a^5F_4-x^5F^\circ_3$	180	20	5
	2999.52	$a^5F_5-x^5F^\circ_5$	340	31	5
	3003.04	$a^5F_3-x^5F^\circ_2$	190	27	5
	3009.58	$a^5F_4-x^5F^\circ_4$	320	36	5
	3016.20	$a^5F_2-x^5F^\circ_1$	160	32	5
	3018.99	$a^5F_3-x^5F^\circ_3$	310	44	4
	3026.47	$a^5F_2-x^5F^\circ_2$	270	54	5
	3031.64	$a^5F_1-x^5F^\circ_1$	220	73	5
	3040.43	$a^5F_4-x^5F^\circ_5$	160	18	5
	3041.75	$a^5F_3-x^5F^\circ_4$	230	33	5
	3042.03	$a^5F_1-x^5F^\circ_2$	130	44	4
	3042.67	$a^5F_2-x^5F^\circ_3$	220	44	5
91.....	3057.45	$a^5F_5-x^5D^\circ_4$	500	46	5
	3067.25	$a^5F_4-x^5D^\circ_3$	520	58	5
	3075.73	$a^5F_3-x^5D^\circ_2$	490	70	5
	3083.75	$a^5F_2-x^5D^\circ_1$	380	76	5
	3091.58	$a^5F_1-x^5D^\circ_0$	270	90	5
	3099.90	$a^5F_1-x^5D^\circ_1$	370	123	5
	3099.97	$a^5F_4-x^5D^\circ_4$	310	34	5
	3100.31	$a^5F_2-x^5D^\circ_2$	390	78	4
	3100.67	$a^5F_3-x^5D^\circ_3$	350	50	4
	3116.64	$a^5F_1-x^5D^\circ_2$	95	32	3

TABLE 1—*Continued*

Mult. No.	λ	Multiplet	*gf*	*f*	No. of Plates
91—*Cont.*	3125.66	$a^5F_2-x^5D^\circ_3$	120	24	3
	3134.11	$a^5F_3-x^5D^\circ_4$	77	11	3
102.....	3143.24	$a^5D_4-z^3F^\circ_3$	0.69	0.077	3
	3180.76	$a^5D_3-z^3F^\circ_2$	3.4	0.68	4
	3184.90	$a^5D_3-z^3F^\circ_3$	6.1	0.87	5
	3193.22	$a^5D_4-z^3F^\circ_4$	6.9	0.77	5
	3199.53	$a^5D_1-z^3F^\circ_2$	2.9	0.97	5
	3214.40	$a^5D_2-z^3F^\circ_3$	5.5	1.10	5
	3236.23	$a^5D_3-z^3F^\circ_4$	6.1	0.87	5
116.....	3191.66	$a^5D_4-z^3D^\circ_3$	5.1	0.57	5
	3196.94	$a^5D_3-z^3D^\circ_2$	4.1	0.59	4
	3200.79	$a^5D_2-z^3D^\circ_1$	0.86	0.17	4
	3229.13	$a^5D_0-z^3D^\circ_1$	2.3	2.3	5
	3234.62	$a^5D_3-z^3D^\circ_3$	3.8	0.54	4
	3245.98	$a^5D_1-z^3D^\circ_2$	4.2	1.4	5
	3265.06	$a^5D_2-z^3D^\circ_3$	3.3	0.66	5
157.....	3452.28	$a^5F_3-y^3F^\circ_4$	66	9.4	2
172.....	3476.71	$a^5D_0-z^5P^\circ_1$	65	65	1
	3497.84	$a^5D_1-z^5P^\circ_2$	23	7.7	1
	3526.07	$a^5D_2-z^5P^\circ_3$	12	2.4	1
183.....	3513.82	$a^5F_5-z^3G^\circ_5$	260	24	6
	3521.26	$a^5F_4-z^3G^\circ_4$	310	35	6
	3526.17	$a^5F_3-z^3G^\circ_3$	180	24	5
	3558.52	$a^5F_2-z^3G^\circ_3$	660	132	6
	3565.38	$a^5F_3-z^3G^\circ_4$	1800	250	2
	3570.10	$a^5F_4-z^3G^\circ_5$	2600	280	1
203.....	3585.32	$a^5F_3-z^5G^\circ_3$	480	69	3
	3585.71	$a^5F_4-z^5G^\circ_4$	260	29	4
	3586.99	$a^5F_2-z^5G^\circ_2$	550	110	6
	3589.11	$a^5F_5-z^5G^\circ_5$	50	4.5	3
	3608.86	$a^5F_1-z^5G^\circ_2$	2000	660	2
3618.78	3618.39	$a^5F_2-z^5G^\circ_3$	2900	590	2
3631.46	~~3641.46~~	$a^5F_3-z^5G^\circ_4$	2000	270	1
	3647.85	$a^5F_4-z^5G^\circ_5$	1600	170	1
257.....	3649.51	$a^5D_4-z^5F^\circ_3$	2.7	0.3	11
	3679.92	$a^5D_4-z^5F^\circ_4$	61	6.8	16
	3683.05	$a^5D_3-z^5F^\circ_2$	9.0	1.3	9
	3705.57	$a^5D_3-z^5F^\circ_3$	110	16	13
	3707.83	$a^5D_2-z^5F^\circ_1$	13	2.6	9
	3719.94	$a^5D_4-z^5F^\circ_5$	530*	59*	7
	3722.56	$a^5D_2-z^5F^\circ_2$	120	24	13
	3733.32	$a^5D_1-z^5F^\circ_1$	92	31	14
	3737.13	$a^5D_3-z^5F^\circ_4$	450*	64	8
	3745.56	$a^5D_2-z^5F^\circ_3$	340	68	8
	3745.90	$a^5D_0-z^5F^\circ_1$	110	110	16
	3748.26	$a^5D_1-z^5F^\circ_2$	190	63	11

TABLE 1—*Continued*

Mult. No.	λ	Multiplet	*gf*	*f*	No. of Plates
276.....	3687.46	$a^5F_5-y^5F^\circ_4$	430	39	7
	3709.25	$a^5F_4-y^5F^\circ_3$	710	79	10
	3727.62	$a^5F_3-y^5F^\circ_2$	760	110	9
	3734.87	$a^5F_5-y^5F^\circ_5$	4700	43	12
	3743.34	$a^5F_2-y^5F^\circ_1$	560	110	8
	3749.49	$a^5F_4-y^5F^\circ_4$	3700	410	13
	3758.24	$a^5F_3-y^5F^\circ_3$	2800	400	13
	3763.79	$a^5F_2-y^5F^\circ_2$	1800	360	11
	3767.19	$a^5F_1-y^5F^\circ_1$	1300	430	10
	3787.88	$a^5F_1-y^5F^\circ_2$	500	170	4
	3795.00	$a^5F_2-y^5F^\circ_3$	590	120	7
	3798.51	$a^5F_4-y^5F^\circ_5$	260	29	5
	3799.55	$a^5F_3-y^5F^\circ_4$	500	72	6
302.....	3786.68	$a^5F_1-z^3P^\circ_0$	37*	12*	7
	3790.10	$a^5F_2-z^3P^\circ_1$	94	19	7
	3812.97	$a^5F_3-z^3P^\circ_2$	330	47	8
	3814.53	$a^5F_1-z^3P^\circ_1$	24*	8.0*	8
	3850.82	$a^5F_2-z^3P^\circ_2$	100	20	8
308.....	3815.84	$a^3F_4-y^3D^\circ_3$	5200	580	8
	3827.83	$a^3F_3-y^3D^\circ_2$	4700	670	8
	3841.05	$a^3F_2-y^3D^\circ_1$	3600	720	8
	3888.52	$a^3F_2-y^3D^\circ_2$	1200	240	7
	3902.95	$a^3F_3-y^3D^\circ_3$	1800	260	8
309.....	3820.43	$a^5F_5-y^5D^\circ_4$	3100	280	16
	3825.88	$a^5F_4-y^5D^\circ_3$	2200	250	16
	3834.23	$a^5F_3-y^5D^\circ_2$	1500	210	11
	3840.44	$a^5F_2-y^5D^\circ_1$	870	170	11
	3849.97	$a^5F_1-y^5D^\circ_0$	510	170	9
	3865.53	$a^5F_1-y^5D^\circ_1$	420	140	9
	3872.50	$a^5F_2-y^5D^\circ_2$	410	82	11
	3878.02	$a^5F_3-y^5D^\circ_3$	420	60	11
	3887.05	$a^5F_4-y^5D^\circ_4$	270	30	10
	3898.01	$a^5F_1-y^5D^\circ_2$	53	19	5
	3917.19	$a^5F_2-y^5D^\circ_3$	42	8.4	4
	3940.88	$a^5F_3-y^5D^\circ_4$	16*	2.3*	5
311.....	3824.44	$a^5D_4-z^5D^\circ_3$	87	9.7	12
	3856.37	$a^5D_3-z^5D^\circ_2$	110	16	12
	3859.91	$a^5D_4-z^5D^\circ_4$	350	39	6
	3878.56	$a^5D_2-z^5D^\circ_1$	88	17.6	12
	3886.28	$a^5D_3-z^5D^\circ_3$	160	23	10
	3895.66	$a^5D_1-z^5D^\circ_0$	52	17	13
	3899.71	$a^5D_2-z^5D^\circ_2$	70	14	13
	3906.48	$a^5D_1-z^5D^\circ_1$	19	6.3	10
	3920.26	$a^5D_0-z^5D^\circ_1$	48	48	13
	3922.91	$a^5D_3-z^5D^\circ_4$	58	8.3	15
	3927.92	$a^5D_1-z^5D^\circ_2$	70	23	16
	3930.30	$a^5D_2-z^5D^\circ_3$	78	16	16
353.....	3969.26	$a^3F_4-y^3F^\circ_3$	1500	170	12
	4005.25	$a^3F_3-y^3F^\circ_2$	1200	170	11
	4045.82	$a^3F_4-y^3F^\circ_4$	6000	670	8

TABLE 1—*Continued*

Mult. No.	λ	Multiplet	*gf*	*f*	No. of Plates
353—*Cont.*	4063.60	$a^3F_3-y^3F^\circ_3$	4300	610	13
	4071.75	$a^3F_2-y^3F^\circ_2$	3800	760	12
	4132.06	$a^3F_2-y^3F^\circ_3$	1100	220	9
	4143.87	$a^3F_3-y^3F^\circ_4$	1400	200	11
418.....	4202.03	$a^3F_4-z^3G^\circ_4$	890	99	18
	4250.79	$a^3F_3-z^3G^\circ_3$	880	130	16
	4271.76	$a^3F_4-z^3G^\circ_5$	2450	270	19
	4307.91	$a^3F_3-z^3G^\circ_4$	3300	470	16
	4325.77	$a^3F_2-z^3G^\circ_3$	3800	760	18
412.....	4206.70	$a^5D_3-z^7P^\circ_3$	0.60	0.086	11
	4216.19	$a^5D_4-z^7P^\circ_4$	2.14	0.24	16
	4258.32	$a^5D_2-z^7P^\circ_3$	0.38*	0.076*	4
	4291.47	$a^5D_3-z^7P^\circ_4$	0.45	0.064	12
448.....	4294.13	$a^3F_4-z^5G^\circ_4$	380	42	6
	4337.05	$a^3F_3-z^5G^\circ_3$	130	19	2
	4383.55	$a^3F_4-z^5G^\circ_5$	5800	650	5
	4404.75	$a^3F_3-z^5G^\circ_4$	3000	430	10
	4415.13	$a^3F_2-z^5G^\circ_3$	1000	200	7
471.....	4347.24	$a^5D_4-z^7F^\circ_4$	0.23*	0.026*	1
	4375.93	$a^5D_4-z^7F^\circ_5$	4.4	0.49	4
	4389.25	$a^5D_3-z^7F^\circ_2$	0.24*	0.034	3
	4427.31	$a^5D_3-z^7F^\circ_4$	4.3	0.61	10
	4435.15	$a^5D_2-z^7F^\circ_1$	0.24*	0.048*	2
	4461.66	$a^5D_2-z^7F^\circ_3$	2.9	0.58	12
	4466.56	$a^5D_1-z^7F^\circ_0$	0.31	0.10	3
	4482.18	$a^5D_1-z^7F^\circ_2$	1.6	0.54	12
	4489.74	$a^5D_0-z^7F^\circ_1$	0.63	0.63	7
508.....	4602.95	$a^3F_4-y^5F^\circ_5$	120	13	1
568.....	5012.07	$a^5F_5-z^5F^\circ_5$	11	1.0	3
580.....	5110.41	$a^5D_4-z^7D^\circ_4$	0.76	0.084	7
	5166.29	$a^5D_4-z^7D^\circ_5$	0.35	0.039	4
	5168.90	$a^5D_3-z^7D^\circ_3$	0.53	0.076	5
	5204.59	$a^5D_2-z^7D^\circ_2$	0.26*	0.052*	3
594.....	5167.49	$a^3F_4-z^3D^\circ_3$	260*	29*	5
	5227.19	$a^3F_3-z^3D^\circ_2$	230*	33*	3
	5270.36	$a^3F_2-z^3D^\circ_1$	180*	36*	3
578.....	5171.60	$a^3F_4-z^3F^\circ_4$	100*	11*	1
604.....	5269.54	$a^5F_5-z^5D^\circ_4$	170	15	9
	5328.04	$a^5F_4-z^5D^\circ_3$	120	13	9
	5371.50	$a^5F_3-z^5D^\circ_2$	80	11	9
	5397.13	$a^5F_4-z^5D^\circ_4$	41	4.6	6
	5405.78	$a^5F_2-z^5D^\circ_1$	58	12	7
	5429.70	$a^5F_3-z^5D^\circ_3$	51	7.3	7
	5434.53	$a^5F_1-z^5D^\circ_0$	34	11	6
	5446.92	$a^5F_2-z^5D^\circ_2$	43	8.6	8
	5455.62	$a^5F_1-z^5D^\circ_1$	35	12	7

linear portion of the curve of growth on any of the spectrograms. Both these multiplets arise from the a^5D term, and their *gf*-values are probably somewhat larger than those for the strong lines of multiplet No. 257. New measures have been included in the results for Nos. 257, 353, 418, and 412, which were published in (1). The relative *gf*-values for a few of the lines of these multiplets have been slightly revised by means of the additional data. These lines are λλ 4045, 4063, and 4071 in No. 353; λλ 4202, 4250, 4271, and 4307 in No. 418; and λλ 4216, 4258, and 4291 in No. 412.

All the *Fe* lines listed were observed in the second order, the first order being used only to connect the lines of the λ 4400 and λ 5200 regions in reducing them to the same scale.

Ti I.—Results for 227 lines in 66 multiplets of *Ti* I between λ 3123 and λ 6743 are listed in Table 2. The relative *gf*-values are on an arbitrary scale, which has, of course, no relation to that for lines of *Fe* I.

As in the case of *Fe* I, all the observed lines arise from the lowest terms, namely, a^3F, a^5F, a^1D, a^3P, b^3F, a^1G, a^5P, a^3G, z^5G^o, b^1G, and a^1P, ranging in excitation potential from 0.0 to 2.5 volts.

In only 33 of the 66 multiplets are the observed intensities complete. The missing lines are all weaker members which did not appear in absorption at the temperatures used.

With the exception of No. 112, which includes both first- and second-order measures, all the multiplets to the red of λ 5100 were measured in the first order. Because of the greater dispersion and resolving power in the second order, measures made there have less uncertainty than those made in the first order.

SOURCES OF ERROR

Sources of error were discussed in (1). It may be emphasized here, however, that in addition to accidental errors inherent in the photographic photometry of faint absorption lines and possible systematic errors due to temperature measurements (and uncertainty in the temperature scale at high temperatures), there are opportunities for the introduction of systematic errors in reducing the measurements from different spectrograms to the same scale. Wide ranges in intensity and in wave length were covered, and in

TABLE 2

RELATIVE *gf*- AND *f*-VALUES FOR LINES OF *Ti* I

Mult. No.	λ	Multiplet	*gf*	*f*	No. of Plates
365.....	3123.07	$a^1D_2-w^1P^\circ_1$	560	112	5
361.....	3141.51	$a^1D_2-x^1P^\circ_1$	440	88	5
347.....	3186.45	$a^3F_2-w^3G^\circ_3$	1200	240	3
	3192.00	$a^3F_3-w^3G^\circ_4$	1750	250	3
	3199.91	$a^3F_4-w^3G^\circ_5$	2300	256	2
	3203.82	$a^3F_3-w^3G^\circ_3$	123	17.6	4
	3214.23	$a^3F_4-w^3G^\circ_4$	134	15	4
	3226.22	$a^3F_4-w^3G^\circ_3$	4.3*	0.48*	5
349.....	3204.87	$a^3P_1-s^3D^\circ_2$	280*	93*	5
343.....	3205.15	$a^3F_2-v^3D^\circ_2$	3.7*	0.74*	5
	3205.85	$a^3F_2-v^3D^\circ_1$	11	2.2	5
	3221.14	$a^3F_3-v^3D^\circ_3$	4.0*	0.57*	5
	3222.74	$a^3F_3-v^3D^\circ_2$	12.2	1.74	5
	3243.80	$a^3F_4-v^3D^\circ_3$	10.5	1.17	5
344.....	3226.11	$z^5G^\circ_6-g^5G^\circ_6$	16000*	1200*	1
336.....	3292.06	$a^1D_2-x^1F^\circ_3$	1060	210	5
334.....	3299.41	$a^1D_2-v^3G^\circ_3$	240*	48*	5
331.....	3308.38	$a^3P_0-t^3D^\circ_1$	560	560	5
	3309.49	$a^3P_1-t^3D^\circ_2$	1300	440	5
	3314.42	$a^3P_2-t^3D^\circ_3$	2200	440	4
	3314.50	$a^3P_1-t^3D^\circ_1$	520	170	3
	3321.58	$a^3P_2-t^3D^\circ_2$	440*	88*	5
320.....	3341.87	$a^3F_2-x^3G^\circ_3$	1080	220	5
	3354.64	$a^3F_3-x^3G^\circ_4$	1570	220	5
	3361.00	$a^3F_3-x^3G^\circ_3$	85	120	9
	3371.44	$a^3F_4-x^3G^\circ_5$	2050	230	5
	3379.20	$a^3F_4-x^3G^\circ_4$	142	16	5
	3385.66	$a^3F_4-x^3G^\circ_3$	84	9.3	9
319.....	3342.14	$a^3F_2-w^3D^\circ_3$	66	13.2	9
	3358.26	$a^3F_2-w^3D^\circ_2$	86	17.2	8
	3361.27	$a^3F_3-w^3D^\circ_3$	120	17.2	5
	3370.42	$a^3F_2-w^3D^\circ_1$	490	98	7
	3377.57	$a^3F_3-w^3D^\circ_2$	690	99	7
	3385.93	$a^3F_4-w^3D^\circ_3$	775	86	7
323.....	3342.70	$a^3F_2-x^5D^\circ_2$	6.4	1.3	5
	3348.52	$a^3F_2-x^5D^\circ_1$	7.4	1.5	5
	3352.92	$a^3F_3-x^5D^\circ_3$	29	4.1	5
	3361.82	$a^3F_3-x^5D^\circ_2$	48	6.9	5
	3377.48	$a^3F_4-x^5D^\circ_3$	570	63	4
315.....	3382.30	$a^3P_2-u^3D^\circ_3$	660	130	5
	3390.67	$a^3P_1-u^3D^\circ_2$	460*	150*	5

TABLE 2—*Continued*

Mult. No.	λ	Multiplet	*gf*	*f*	No. of Plates
304.....	3480.53	$a^3P_2-w^3P^\circ_2$	550	110	5
302.....	3493.27	$a^3F_3-y^5F^\circ_4$	6.7	0.96	5
	3506.64	$a^3F_4-y^5F^\circ_5$	22	2.45	5
288.....	3603.86	$a^3F_2-z^5P^\circ_2$	2.4*	0.48*	5
	3606.81	$a^3F_3-z^5P^\circ_3$	6.2	0.89	11
	3626.09	$a^3F_3-z^5P^\circ_2$	6.1	0.87	11
	3635.20	$a^3F_4-z^5P^\circ_3$	26	2.9	11
294.....	3604.30	$a^3F_3-y^1D^\circ_2$	9.1	1.3	11
291.....	3610.16	$a^1D_2-y^1P^\circ_1$	850	170	11
284.....	3635.47	$a^3F_2-y^3G^\circ_3$	1600	320	7
	3642.68	$a^3F_3-y^3G^\circ_4$	1900	270	7
	3653.49	$a^3F_4-y^3G^\circ_5$	2500	280	6
	3658.14	$a^3F_3-y^3G^\circ_3$	117	17	10
	3671.66	$a^3F_4-y^3G^\circ_4$	121	13.5	10
	3687.38	$a^3F_4-y^3G^\circ_3$	9.6	1.1	11
283.....	3637.97	$a^3F_2-x^3D^\circ_3$	19	3.8	11
	3646.19	$a^3F_2-x^3D^\circ_2$	40	8.0	14
	3654.58	$a^3F_2-x^3D^\circ_1$	62	12.4	17
	3660.62	$a^3F_3-x^3D^\circ_3$	58	8.3	16
	3668.95	$a^3F_3-x^3D^\circ_2$	71	10.1	17
	3689.89	$a^3F_4-x^3D^\circ_3$	78	8.7	17
276.....	3702.29	$a^3P_0-y^3S^\circ_1$	250*	250*	3
	3709.95	$a^3P_1-y^3S^\circ_1$	610	200	10
	3725.12	$a^3P_2-y^3S^\circ_1$	970	194	11
271.....	3717.39	$a^3F_2-x^3F^\circ_3$	81	16	9
	3722.58	$a^3F_3-x^3F^\circ_4$	95	14	5
	3729.77	$a^3F_2-x^3F^\circ_2$	690	140	8
	3741.06	$a^3F_3-x^3F^\circ_3$	1000	150	4
	3752.87	$a^3F_4-x^3F^\circ_4$	1700	190	4
	3753.63	$a^3F_3-x^3F^\circ_2$	122	17.5	10
	3771.64	$a^3F_4-x^3F^\circ_3$	129	14.3	10
277.....	3724.59	$a^1G_4-x^1G^\circ_4$	3400	380	8
269.....	3786.03	$a^1D_2-z^1P^\circ_1$	1450	290	6
249.....	2889.96	$a^3F_2-y^5D^\circ_2$	7.7	1.5	6
	3900.96	$a^3F_3-y^5D^\circ_3$	46	6.6	7
	3914.33	$a^3F_4-y^5D^\circ_4$	75	8.3	9
	3934.23	$a^3F_4-y^5D^\circ_3$	9.6	10.7	6
246.....	3898.49	$a^3F_2-y^3D^\circ_3$	11.6	2.3	6
	3924.51	$a^3F_3-y^3D^\circ_3$	180	26	6
	3929.87	$a^3F_2-y^3D^\circ_2$	132	26	6
	3948.66	$a^3F_2-y^3D^\circ_1$	590	120	5
	3956.28	$a^3F_3-y^3D^\circ_2$	610	87	5
	3958.21	$a^3F_4-y^3D^\circ_3$	1120	125	5

TABLE 2—*Continued*

Mult. No.	λ	Multiplet	*gf*	*f*	No. of Plates
255.....	3904.77	$a^1D_2-y^1F^\circ_3$	2300	460	6
247.....	3914.72	$a^3F_2-z^3P^\circ_1$	4.6*	0.92*	6
	3921.42	$a^3F_2-z^3P^\circ_2$	44	8.8	6
	3947.75	$a^3F_3-z^3P^\circ_2$	167	24	6
239.....	3962.85	$a^3F_2-y^3F^\circ_3$	105	21	6
	3964.27	$a^3F_3-y^3F^\circ_4$	105	15	6
	3981.77	$a^3F_2-y^3F^\circ_2$	770	154	7
	3989.77	$a^3F_3-y^3F^\circ_3$	1090	156	7
	3998.65	$a^3F_4-y^3F^\circ_4$	1700	190	7
	4008.94	$a^3F_3-y^3F^\circ_2$	151	22	8
	4024.57	$a^3F_4-y^3F^\circ_3$	164	18	6
243.....	3982.54	$a^3F_2-z^5S^\circ_2$	78	15.6	11
	4009.68	$a^3F_3-z^5S^\circ_2$	32	4.6	8
233.....	4055.02	$a^3P_0-x^3P^\circ_1$	290*	290*	6
	4060.27	$a^3P_1-x^3P^\circ_2$	370*	120*	6
	4064.22	$a^3P_1-x^3P^\circ_1$	250*	83*	4
	4065.11	$a^3P_1-x^3P^\circ_0$	290*	97*	6
	4078.47	$a^3P_2-x^3P^\circ_2$	1070	210	4
	4082.46	$a^3P_2-x^3P^\circ_1$	320	64	5
231.....	4076.38	$a^3F_3-z^1G^\circ_4$	2.0*	0.29*	1
	4112.73	$a^3F_4-z^1G^\circ_4$	40	45	6
209.....	4272.44	$a^5F_3-x^5D^\circ_4$	70*	10*	2
	4274.60	$a^5F_2-x^5D^\circ_3$	106*	21*	5
	4281.40	$a^5F_1-x^5D^\circ_2$	110	37	5
	4286.01	$a^5F_3-x^5D^\circ_3$	780	110	10
	4287.41	$a^5F_4-x^5D^\circ_4$	780	86	10
	4289.08	$a^5F_2-x^5D^\circ_2$	950	190	10
	4290.93	$a^5F_{4,3}-x^5D^\circ_{3,2}$	680	230	10
	4295.75	$a^5F_1-x^5D^\circ_0$	740	250	10
	4298.67	$a^5F_2-x^5D^\circ_1$	1310	260	10
	4300.55	$a^5F_3-x^5D^\circ_2$	2100	300	4
	4301.08	$a^5F_4-x^5D^\circ_3$	2600	290	4
	4305.91	$a^5F_5-x^5D^\circ_4$	4600	420	3
204.....	4299.64	$a^5F_3-w^3D^\circ_3$	240	34	8
	4314.80	$a^5F_2-w^3D^\circ_2$, $a^5F_4-w^3D^\circ_3$	780	.....	9
	4326.35	$a^5F_3-w^3D^\circ_2$	140*	20*	3
181.....	4465.80	$a^5P_2-y^5P^\circ_3$	1400*	280*	2
	4471.24	$a^5P_1-y^5P^\circ_2$	1500*	500*	2
	4481.27	$a^5P_3-y^5P^\circ_3$	2800*	400*	3
	4489.10	$a^5P_2-y^5P^\circ_1$	1800*	360*	2
172.....	4512.74	$a^5F_4-y^5F^\circ_5$	550	61	13
	4518.03	$a^5F_3-y^5F^\circ_4$	750	107	12
	4522.80	$a^5F_2-y^5F^\circ_3$	740	148	12
	4527.32	$a^5F_1-y^5F^\circ_2$	520	173	13

TABLE 2—*Continued*

Mult. No.	λ	Multiplet	*gf*	*f*	No. of Plates
172—*Cont.*	4533.25	$a^5F_5 - y^5F^\circ_5$	5100	460	6
	4534.78	$a^5F_4 - y^5F^\circ_4$	3500	390	5
	4535.58	$a^5F_3 - y^5F^\circ_3$	1900	270	4
	4535.92	$a^5F_2 - y^5F^\circ_2$	1180	240	10
	4536.00	$a^5F_1 - y^5F^\circ_1$	910	300	12
	4544.70	$a^5F_2 - y^5F^\circ_1$	500	100	13
	4548.72	$a^5F_3 - y^5F^\circ_2$	735	105	14
	4552.45	$a^5F_4 - y^5F^\circ_3$	755	84	12
	4555.50	$a^5F_5 - y^5F^\circ_4$	550	50	13
169.....	4562.63	$a^3F_3 - z^1D^\circ_2$	3.6	0.51	4
163.....	4617.27	$a^5P_3 - w^5D^\circ_4$	3400	490	5
	4623.10	$a^5P_2 - w^5D^\circ_3$	1700*	350*	5
	4639.36	$a^5P_2 - w^5D^\circ_2$	1500*	300*	2
	4639.66	$a^5P_3 - w^5D^\circ_3$	1300*	180*	1
157.....	4656.47	$a^3F_2 - z^3G^\circ_3$	70	14	8
	4667.59	$a^3F_3 - z^3G^\circ_4$	91	13	8
	4681.91	$a^3F_4 - z^3G^\circ_5$	132	14.7	8
	4693.68	$a^3F_3 - z^3G^\circ_3$	2.6	0.37	5
	4715.31	$a^3F_4 - z^3G^\circ_4$	2.4	0.27	5
162.....	4675.13	$a^3P_2 - x^5D^\circ_3$	71*	14*	2
155.....	4691.34	$a^3P_2 - w^3D^\circ_3$	210	42	5
	4698.79	$a^3P_1 - w^3D^\circ_2$	160	54	4
	4710.19	$a^3P_0 - w^3D^\circ_1$	80*	80*	4
	4722.63	$a^3P_1 - w^3D^\circ_1$	66*	22*	2
143.....	4840.88	$a^1D_2 - y^1D^\circ_2$	460	92	6
138.....	4885.09	$a^3G_5 - y^3H^\circ_6$	3400*	310*	4
	4899.93	$a^3G_4 - y^3H^\circ_5$	2600*	290*	3
	4913.63	$a^3G_3 - y^3H^\circ_4$	2500*	360*	2
128.....	4981.75	$a^5F_5 - y^5G^\circ_6$	5200	470	6
	4991.08	$a^5F_4 - y^5G^\circ_5$	4000	440	6
	4999.51	$a^5F_3 - y^5G^\circ_4$	3150	450	5
	5007.22	$a^5F_2 - y^5G^\circ_3$	2100	420	4
	5014.28	$a^5F_1 - y^5G^\circ_2$	1600	540	4
	5016.17	$a^5F_5 - y^5G^\circ_5$	460	42	6
	5020.04	$a^5F_4 - y^5G^\circ_4$	640	71	6
	5022.87	$a^5F_3 - y^5G^\circ_3$	590	84	6
	5024.85	$a^5F_2 - y^5G^\circ_2$	410	82	6
126.....	4997.10	$a^3F_2 - z^3D^\circ_2$	12	2.4	6
	5009.65	$a^3F_3 - z^3D^\circ_3$	8.9	1.3	6
	5014.19	$a^3F_2 - z^3D^\circ_1$	94	19	6
	5039.96	$a^3F_3 - z^3D^\circ_2$	135	19	6
	5064.66	$a^3F_4 - z^3D^\circ_3$	180	20	5
123.....	5035.92	$b^3F_4 - w^3G^\circ_5$	2500	280	5
	5036.47	$b^3F_3 - w^3G^\circ_4$	1950	280	5
	5038.41	$b^3F_2 - w^3G^\circ_3$	1550	310	5

TABLE 2—*Continued*

Mult. No.	λ	Multiplet	*gf*	*f*	No. of Plates
119.....	5113.45	$b^3F_3-v^3D^\circ_2$	420	60	4
	5145.47	$b^3F_4-v^3D^\circ_3$	670	74	10
112.....	5147.48	$a^3F_2-z^3F^\circ_3$	14.7	2.9	12
	5152.18	$a^3F_3-z^3F^\circ_4$	14.4	2.1	12
	5173.74	$a^3F_2-z^3F^\circ_2$	135	27	5
	5192.98	$a^3F_3-z^3F^\circ_3$	180	26	5
	5210.39	$a^3F_4-z^3F^\circ_4$	240	25	4
	5219.72	$a^3F_3-z^3F^\circ_2$	7.7	1.1	11
	5252.11	$a^3F_4-z^3F^\circ_3$	4.8	0.53	5
115.....	5206.09	$a^1P_1-w^1P^\circ_1$	16500	5500	1
113.....	5238.58	$a^5F_5-y^5D^\circ_4$	31	2.8	7
	5246.56	$a^5F_4-y^5D^\circ_3$	17.5	1.95	7
	5250.94	$a^5F_3-y^5D^\circ_2$	12*	1.8*	5
105.....	5265.97	$a^3G_5-v^3F^\circ_4$	1100	100	3
	5283.45	$a^3G_4-v^3F^\circ_3$	930	100	2
	5297.29	$a^3G_3-v^3F^\circ_2$	860	120	3
103.....	5282.38	$a^3P_1-x^3D^\circ_2$	42	14	3
	5284.39	$a^3P_0-x^3D^\circ_1$	30	30	2
	5295.78	$a^3P_2-x^3D^\circ_3$	68	13.6	10
98.....	5366.63	$a^5F_2-y^3F^\circ_3$	11*	2.2*	1
	5389.15	$a^5F_1-y^3F^\circ_2$	9.1*	3.0*	2
91.....	5396.57	$a^3F_3-z^5D^\circ_4$, $a^3F_2-z^5D^\circ_2$	1.24	.....	10
	5408.93	$a^3F_2-z^5D^\circ_1$	0.38*	0.076*	2
	5426.27	$a^3F_3-z^5D^\circ_3$	2.55	0.36	10
	5446.67	$a^3F_3-z^5D^\circ_2$	1.01	0.144	10
	5460.51	$a^3F_4-z^5D^\circ_4$	3.7	0.41	10
	5490.82	$a^3F_4-z^5D^\circ_3$	0.99	0.11	7
94.....	5474.28	$b^3F_4-x^3G^\circ_5$	140*	16*	4
88.....	5481.90	$b^3F_2-w^3D^\circ_2$	140*	28*	4
	5512.54	$b^3F_4-w^3D^\circ_3$	840	93	10
	5514.36	$b^3F_2-w^3D^\circ_1$	640	128	10
	5514.54	$b^3F_3-w^3D^\circ_2$	860	123	10
92.....	5490.16	$b^3F_4-x^5D^\circ_3$	300	33	7
84.....	5644.14	$b^1G_4-y^1G^\circ_4$	3300	370	1
72.....	5866.45	$a^3P_2-y^3D^\circ_3$	265	53	9
	5899.29	$a^3P_1-y^3D^\circ_2$	157	52	10
	5922.11	$a^3P_0-y^3D^\circ_1$	75	75	9
	5941.73	$a^3P_1-y^3D^\circ_1$	57	19	8
73.....	5880.30	$a^3P_1-z^3P^\circ_2$	30	10	1
	5918.56	$a^3P_2-z^3P^\circ_2$	50	10	7

TABLE 2—*Continued*

Mult. No.	λ	Multiplet	*gf*	*f*	No. of Plates
70.....	5953.16	$a^3G_5-z^3H^\circ_6$	1100	100	3
	5965.83	$a^3G_4-z^3H^\circ_5$	1000	110	4
	5978.54	$a^3G_3-z^3H^\circ_4$	850	120	2
60.....	6064.64	$a^3P_0-z^3S^\circ_1$	30	30	3
	6085.22	$a^3P_1-z^3S^\circ_1$	64	21	10
	6126.21	$a^3P_2-z^3S^\circ_1$	82	16	10
54.....	6258.10	$b^3F_3-y^3G^\circ_4$	670	96	10
	6258.70	$b^3F_4-y^3G^\circ_5$	875	97	10
	6261.10	$b^3F_2-y^3G^\circ_3$	560	112	10
48.....	6546.26	$b^3F_2-x^3F^\circ_2$	120*	24*	2
	6554.23	$b^3F_3-x^3F^\circ_3$	120*	17*	4
	6556.08	$b^3F_4-x^3F^\circ_4$	155	17	4
46.....	6599.12	$a^1D_2-z^1F^\circ_3$	15	3.1	4
43.....	6743.14	$a^1D_2-z^1D^\circ_2$	48	9.6	1

some cases two sets of data had only a few lines in common for the determination of the reduction factors. Hence systematic errors with respect to both intensity and wave length may be present. It may be possible to detect these errors by observations of emission spectra, since for such spectra a larger range of intensity can be measured on a single spectrogram. Furnace emission spectra will also extend the observations to lines of higher excitation potential. The absorption spectrum method, while more favorable for the measurement of intensities of lines arising from the lowest levels, is limited to such lines.

Our thanks are due to Miss Dorothy Carlson, who made a large number of the microphotometer tracings.

MASSACHUSETTS INSTITUTE OF TECHNOLOGY,
CARNEGIE INSTITUTION OF WASHINGTON
MOUNT WILSON OBSERVATORY
August 1937

TEMPERATURE IN THE SOLAR REVERSING LAYER DERIVED FROM TITANIUM LINES

ROBERT B. KING

ABSTRACT

A temperature for the solar reversing layer is derived by a comparison of the equivalent widths of solar *Ti* I lines with laboratory *gf*-values. Boltzmann factors for lines arising from different low-energy levels are found by plotting solar equivalent widths as a function of *gf*. These give a mean temperature of 4400° K.

An empirical curve of growth for the sun is constructed with the aid of the temperature thus found and the laboratory *gf*-values for *Fe* I and *Ti* I.

Comparison of the data on relative *gf*-values for lines of *Fe* I and *Ti* I given in the preceding paper[1] with the equivalent widths of these lines in the solar spectrum leads to a temperature for the solar reversing layer. Extensive measures of equivalent widths of solar absorption lines in the region λλ 4036–6600 have been made by C. W. Allen,[2] including many of the lines whose relative *gf*-values have been determined in the laboratory.

The problem of determining a temperature for the reversing layer from these data is simply a matter of finding the Boltzmann factor to be applied to the laboratory data which will bring the relative intensities of the lines arising from different energy levels into agreement with their relative intensities observed in the solar spectrum. The relative numbers of atoms in two levels of energies, E_1 and E_2, at a temperature T is given by the Boltzmann formula

$$\frac{N_2}{N_1} = \frac{e^{-E_2/KT}}{e^{-E_1/KT}} \frac{g_2}{g_1}, \tag{1}$$

where g_1 and g_2 are the statistical weights of the levels. Taking only the temperature factor into account, we have

$$\frac{N_2}{N_1} = e^{-\frac{hc}{KT}\Delta\nu}, \tag{2}$$

[1] R. B. King and A. S. King, *Mt. W. Contr.*, No. 581; *Ap. J.*, **87**, 24, 1938.

[2] *Mem. Commonwealth Solar Obs., Canberra*, Australia, No. 5, 1935.

where $\Delta\nu$ is the wave-number difference between the two levels. This can be written in the form (logarithm to base 10)

$$\log R = -\frac{0.625\Delta\nu}{T} \tag{3}$$

where R is the Boltzmann factor and $\log R$ is to be added to values of $\log gf$ to allow for a temperature distribution of atoms among the various low levels from which the absorption lines arise. If solar values of $\log EW/\lambda^2$ are plotted against relative values of $\log gf$ for these lines, then all the lines arising from the same low level should fall on the same curve of growth. The displacement of the curves of growth for different low levels will be a measure of $\log R$, and hence of the temperature in the part of the atmosphere where the lines are formed. It must be assumed, of course, that conditions there approximate thermal equilibrium, if the temperatures derived from Boltzmann factors are to have meaning.

Although laboratory and solar data for lines of both *Fe* I and *Ti* I are available, only those for *Ti* I are suitable for this purpose. The *Fe* lines, unfortunately, lie for the most part on the transition portion of the solar curve of growth, between the linear and radiation-damping portions, in a region dominated by Doppler effect. Since here $EW \propto \sqrt{Nf + C}$, the displacements of curves of growth for lines arising from different levels along the $\log gf$ co-ordinate cannot be determined with any degree of precision. The *Ti* data, however, are well suited for this purpose. The lines are all faint in the sun, and many lie on the linear portion of the curves of growth, where displacements are readily measured.

Figure 1 shows a plot of $\log EW/\lambda^2$ for the sun against laboratory values of $\log gf$ for lines of *Ti* I. The values of $\log gf$ have been reduced to the lowest sublevel of the low state from which they arise for a temperature of 4500° K. That is, all the lines arising from the $b^3F_{2,3,4}$ sublevels, for example, have been reduced to the b^3F_2 sublevel, which is 11,531 wave-numbers above the 0.0 level a^3F_2. All lines from the b^3F levels should therefore fall on the same curve of growth. Lines known to be blends in the solar spectrum were excluded.

There is some question[2] as to how the solar equivalent widths vary with wave length. The present data do not appear to be complete or precise enough to settle this point. Plotting equivalent widths as various other functions of the wave length alters the scatter of the points but does not reveal systematic trends clearly enough to warrant any conclusions. The curves of growth defined by such plots are very nearly the same as those in Figure 1, and the mean temperature derived from them is not appreciably different.

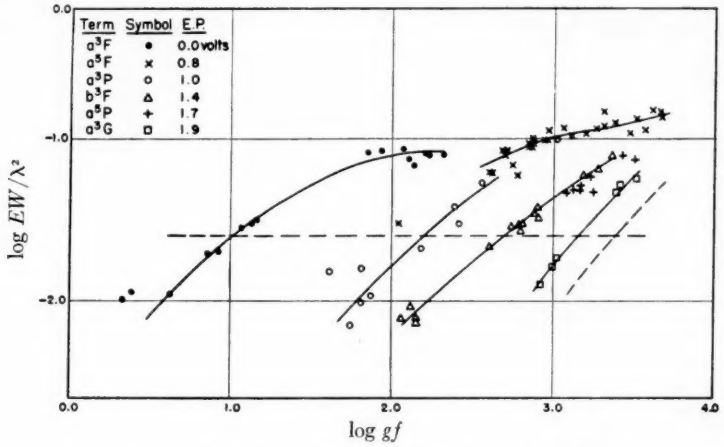

FIG. 1.—log EW/λ^2 (Sun) as a function of log gf (Lab.)

In Figure 1 the displacements of the curves of growth from that for the a^3F level, measured along the horizontal dotted line, give values of log R. Only the curves for lines from the a^3P, b^3F, and a^3G levels were regarded as suitable for the purpose. The results are shown in

Level	$\Delta\nu$	log R	T
a^3P.....	8436	−1.18	4470° K
b^3F.....	11531	−1.67	4310
a^3G.....	15108	−2.14	4420

the table, where $\Delta\nu$ is the wave-number difference between the lowest sublevel and a^3F_2. The absolute temperature T is derived by means of equation (3). The resulting mean temperature is 4400° K with an estimated uncertainty of the order of ±100°. The dotted

line on the right in Figure 1 gives an indication of the degree of precision. This would be the position of the curve for a^3G relative to that for a^3F if the temperature were 4000° K. Since the laboratory *gf*-values depend on measures with an optical pyrometer of furnace temperatures of 1800°–2600° C, the solar temperature derived here depends largely on these measures. Any error in laboratory temperature scale and any possible departure from thermal equilibrium in the furnace enter into the results.

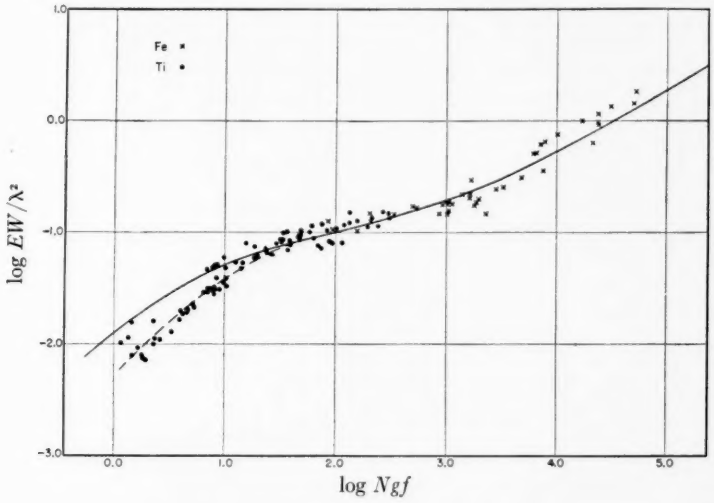

FIG. 2.—Curve of growth for the Sun

It is noteworthy that no assumption need be made as to the form of the solar curve of growth, since the temperatures were derived from the displacements of empirical curves.

The laboratory and solar data, together with the temperature derived here, enable one to construct an empirical curve of growth for the sun. This curve is shown in Figure 2, where values of log EW/λ^2 (reduced to λ 5000) are plotted against laboratory values of log Ngf, a temperature of 4400° K being used to determine relative values of N. The data for *Fe* and *Ti* were plotted separately and superposed as accurately as possible by shifting the two plots horizontally. The full-line curve is a theoretical curve of growth for the sun used by Allen.[2] It is unfortunate that neither the *Fe* nor the *Ti*

data extend over the whole course of the curve from linear to damping portions. Hence a good check on the value of the damping constant cannot be obtained. There is no indication, however, of wide departure (except on the linear portion) from Allen's theoretical curve calculated on the assumption of a value ten times the classical value of this constant.

Measurements of the temperature of the solar reversing layer by means of spectroscopic relations involving the temperature have been few because of the lack of data for both laboratory and solar-line intensities. Real differences in such determinations might be expected if the spectra of vapors which absorb most effectively at very different atmospheric levels were examined. The temperature derived by Birge ($4300° \pm 500°$ K)[3] and that of Richardson ($5700° \pm 1600°$ K)[4] from the intensity distributions in the solar bands of *CN* λ 3883 and C_2 λ 5165, respectively, may be mentioned in connection with the foregoing result derived from neutral titanium lines.

MASSACHUSETTS INSTITUTE OF TECHNOLOGY
CAMBRIDGE, MASSACHUSETTS
September 1937

[3] *Ap. J.*, **55**, 273, 1922.

[4] *Mt. W. Contr.*, No. 422; *Ap. J.*, **73**, 216, 1931.

THE EFFECT OF AN ADIABATIC LAYER UPON SOLAR LIMB DARKENING

PHILIP C. KEENAN

ABSTRACT

On the assumption that there exists a zone of instability characterized by an adiabatic temperature gradient beginning at optical depth τ_1 below the surface of the photosphere, the boundary conditions determine the distribution of temperature within the unstable layer. The limb darkening can then be determined for different values of τ_1 and computations carried out for boundaries of 1.0, 0.67, 0.50, and 0.28 predict curves of darkening similar in character to the observed curve. However, an appreciable effect due to the adiabatic layer could occur only if its upper boundary were considerably higher than the optical depth of two now generally assigned to it.

According to the criterion of stability derived originally by Schwarzschild,[1] an atmosphere in radiative equilibrium will be mechanically stable if its temperature gradient,

$$\left(\frac{dT}{dh}\right)_{\text{rad}},$$

is less than that in an adiabatic atmosphere. Unsöld[2] has shown that on the assumption of an opacity law of the form $\kappa \sim p^n$, the condition for stability corresponds to the inequality

$$1 - \frac{T_0^4}{T^4} < \frac{4(\gamma - 1)}{(n + 1)\gamma}. \qquad (1)$$

When the value of γ, the ratio of specific heats, is so low that the inequality is reversed, the atmosphere is unstable and convection currents will develop and presumably transport sufficient quantities of heat to establish adiabatic equilibrium within the zone of instability.[3] Accepting for the present Siedentopf's conclusion that the convection currents will transport so little energy above the zone of instability that radiative equilibrium will be re-established within a very short distance,[4] the inequality (1) when written as an

[1] *Göttingen Nachrichten*, p. 41, 1906.

[2] *Zs. f. Ap.*, **1**, 138, 1930.

[3] See the discussion by H. H. Plaskett, *M.N.*, **96**, 402, 1936.

[4] *A.N.*, **255**, 157, 1935.

equation defines the temperature T_1 at the junction of the adiabatic and radiative layers.

Since

$$T_1^4 = T_0^4(1 + \tfrac{3}{2}\tau_1)\,, \tag{2}$$

we have for the optical depth corresponding to the upper boundary of the convective layer

$$\frac{\frac{3}{2}\tau_1}{1 + \frac{3}{2}\tau_1} = \frac{4(\gamma - 1)}{(n + 1)\gamma} \tag{3}$$

or

$$\tau_1 = \frac{8}{3}\frac{\gamma - 1}{4 - (3 - n)\gamma}\,, \tag{4}$$

defining the optical depth at which instability will be just setting in for a given value of γ (we shall assume that γ is constant in the adiabatic zone). The effective ratio of specific heats at any depth depends upon the rate at which the various gases are being ionized. Computations carried out by Unsöld[2] and by Siedentopf[4] show that the zone of instability in the sun begins at $\tau \approx 2$ and extends inward to an optical depth of about 300, i.e., over a distance of several hundred kilometers.

The possibility that this region of convection influences the limb darkening at the surface has led Plaskett[3] to attempt to derive the solar temperature distribution directly from the accurate observations of darkening in different parts of the spectrum made by Moll, Burger, and van der Bilt on the Gornergrat in Switzerland.[5] Taking their data for λ 5500, Plaskett employed an approximate summation to solve the integral equation for $B_\lambda(\tau)$ in terms of the intensity of the emergent radiation. He found a distortion of the radiative temperature distribution in the form of a nearly isothermal region near $\tau = 1$, followed by a gradient steeper than the radiative near the surface (see Fig. 7 of his paper). From this result Plaskett concluded that the observations indicated the presence of an unstable layer of the sort predicted.

However, the deduced temperature distribution is inconsistent with that which must prevail in such an adiabatic layer, where the

[5] *B.A.N.*, **3**, 83, 1925.

temperature gradient is at all points less than the radiative gradient. Furthermore, although this is undoubtedly an accurate solution of the equations, it is by no means obvious that it is the only temperature distribution which will fit the data within the quite appreciable observational uncertainty.

Some of this ambiguity may be removed by approaching the problem from a different direction, in accordance with a suggestion made by Chandrasekhar. Consider an atmosphere containing a layer in adiabatic equilibrium with its upper boundary at a specified optical depth τ_1 and extending inward to a depth so great that the matter beyond it will not contribute appreciably to the surface radiation. What will be the observed limb darkening for different values of τ_1?

There will be one definite curve of darkening for each τ_1 if the temperature distribution within the convective layer is uniquely determined by τ_1, and we shall see that this is actually the case.

Starting with the equation of hydrostatic equilibrium,

$$dp = g\rho\, dx \qquad (x \text{ increasing inward}), \tag{5}$$

and the defining equation for τ,

$$d\tau = \kappa\rho\, dx, \tag{6}$$

we have

$$d\tau = \frac{\kappa}{g}\, dp. \tag{7}$$

Introducing an opacity law of the form

$$\kappa = \kappa_0 p^n \tag{8}$$

and integrating, we obtain

$$\frac{g}{\kappa_0}(\tau + D) = \frac{p^{n+1}}{n+1}$$

or

$$p = \left[\frac{(n+1)g}{\kappa_0}\right]^{\frac{1}{n+1}} (\tau + D)^{\frac{1}{n+1}}, \tag{9}$$

where D is a constant of integration.

We now introduce the adiabatic condition in the form

$$T = C_1 p^{\frac{\gamma-1}{\gamma}} . \tag{10}$$

Substituting from (9), and writing $B_A(\tau)$ for the emissivity within the adiabatic region, we find

$$\begin{aligned} B_A(\tau) = \frac{\sigma}{\pi} T^4 = \frac{\sigma}{\pi} C_1^4 \left[\frac{(n+1)g}{\kappa_0}\right]^{\frac{4(\gamma-1)}{(n+1)\gamma}} \cdot (\tau + D)^{\frac{4(\gamma-1)}{(n+1)\gamma}} \\ = CB_R(0)[\tau + D]^q , \end{aligned} \tag{11}$$

where $q = 4(\gamma - 1)/(n + 1)\gamma$ and $B_R(0)$, the emissivity at $\tau = 0$, is introduced into the multiplying constant for convenience in computation.

For a specified τ_1 the constants C and D are determined by the following boundary conditions:

1. At τ_1, $B_A(\tau_1) = B_R(\tau_1)$,

where

$$B_R(\tau) = B_R(0)[1 + \tfrac{3}{2}\tau] . \tag{12}$$

Combining equations (11) and (12), the condition becomes

$$C = \frac{(1 + \tfrac{3}{2}\tau_1)}{(\tau_1 + D)^q} . \tag{13}$$

2. At τ_1 the net flux must be equal to the observed net flux (F) at the surface of the sun.

$$\frac{F}{\pi} = 2B_R(0) = \frac{F_+}{\pi} - \frac{F_-}{\pi} . \tag{14}$$

The inward flux due to the upper layer in radiative equilibrium can be readily determined from the equation[6]

$$\frac{F_-}{\pi} = \tfrac{3}{2}\tau_1 B_R(0) - 2B_R(0) \int_0^{\pi/2} \cos\psi \sin\psi e^{-\tau_1 \sec\psi} (1 - \tfrac{3}{2}\cos\psi) d\psi .$$

[6] See Milne, *Handbuch d. Ap.*, **3**, 128, eq. (151), 1930.

Using the substitution $y = \tau_1 \sec \psi$, the solution comes out in terms of the exponential integral as

$$\frac{F_-}{\pi} = B_R(0)\left[\tfrac{3}{2}\tau_1 + \tfrac{1}{2}\tau_1 e^{-\tau_1} + \tfrac{1}{2}\tau_1^2 e^{-\tau_1} + \left(\tau_1^2 + \frac{\tau_1^3}{2}\right)E_i(-\tau_1)\right]. \quad (15)$$

In order to evaluate the outward stream of radiation at τ_1, we assume that γ is constant within the convective layer. Then

$$I_+(\tau_1, \theta) = \int_{\tau_1}^{\infty} e^{(\tau_1 - \tau)\sec\theta} B_A(\tau) \cdot \sec\theta \cdot d\tau . \quad (16)$$

Substituting for $B_A(\tau_1)$ from (11) and writing $\tau = t\cos\theta - D$,

$$I_+(\tau_1, \theta) = CB_R(0)e^{(\tau_1 + D_1)\sec\theta}(\cos\theta)^q[\Gamma(q+1) - \Gamma_D(q+1)]$$

and

$$\frac{F_+}{\pi} = 2CB_R(0)\int^{\tau_1} (\cos\theta)^{q+1} e^{(\tau_1 + D)\sec\theta}[\Gamma(q+1) - \Gamma_D(q+1)]d(\cos\theta) , \quad (17)$$

where $\Gamma_D\,(q+1)$ is the incomplete gamma function[7]

$$\int_0^{(\tau_1 + D)\sec\theta} t^q e^{-t} dt .$$

Solution of (17) by graphical integration is convenient and accurate, since the integrand decreases almost linearly with $\cos\theta$. If we write $\sec\theta = x$ and $\tau_1 + D = a$, it may be shown that[8]

$$\lim_{x\to\infty} \frac{e^{ax}[\Gamma(q+1) - \Gamma_D(q+1)]}{x^{q+1}} \sim \frac{1}{x} .$$

Since the unknown D is involved in the integral, it is necessary to determine the constants by successive approximations. However, three integrations have usually been found to give sufficiently accurate values.

With the constants known the complete temperature distribution is fixed, and the limb darkening can be found directly. Adding the

[7] K. Pearson, *Tables of the Incomplete* Γ*-Function*, Cambridge, 1934.

[8] See Whittaker and Watson, *Modern Analysis* (3d ed., 1920), p. 341.

contributions from the two layers, we have for the emergent radiation

$$I(0, \theta) = \int_0^{\tau_1} B_R(\tau) e^{-\tau \sec\theta} \sec\theta \cdot d\tau + \int_{\tau_1}^{\infty} B_A(\tau) e^{-\tau \sec\theta} \sec\theta \cdot d\tau .$$

Substituting for $B_R(\tau)$ and $B_A(\tau)$ and integrating,

$$\begin{aligned} I(0, \theta) = {} & B_R(0)[1 + \tfrac{3}{2}\cos\theta - e^{-\tau_1 \sec\theta}(1 + \tfrac{3}{2}\tau_1 + \tfrac{3}{2}\cos\theta)] \\ & + B_R(0) \cdot C \cdot e^{D \sec\theta}(\cos\theta)^q[\Gamma(q+1) - \Gamma_D(q+1)] . \end{aligned} \qquad (18)$$

For $\tau_1 = \infty$ the equation reduces to the cosine law of radiative equilibrium, while for $\tau_1 = 0$ we obtain the well-known result that an adiabatic atmosphere shows complete darkening at the limb.

It is important to note that the darkening for a given value of τ_1 is independent of the coefficient n in the opacity law. This follows from the fact that n and λ enter the expressions for the constants only through q, and by equation (3)

$$q = \frac{\frac{3}{2}\tau_1}{1 + \frac{3}{2}\tau_1} \qquad (19)$$

for all values of n.

By means of the foregoing equations the solar limb darkening that would result from an adiabatic layer beginning at any specified optical depth can be determined. Computations have been carried out for $\tau_1 = 1.0, 0.67$, and 0.28 in turn. As an example of the numerical values, for $\tau_1 = 1.0$; $q = 0.6$, $D = -0.18$, and $C = 2.82$.

The resulting curves of darkening for the three cases are plotted as the broken lines in Figure 1. The straight line shows the normal cosine darkening for an atmosphere in complete radiative equilibrium. For comparison the observations of Abbott, Fowle, and Aldrich as reduced to integrated light by Lindblad[9] are represented on the diagram by filled circles.

Since the diminished temperature gradient in the adiabatic layer lying below the surface weakens the intensity of the light observed at the center of the disk but does not influence the radiation from

[9] *Nova Acta Reg. Soc. Sc. Upsal.*, **6**, No. 1, 17, 1923.

the limb, the effect of the unstable region is to reduce limb darkening over the greater part of the sun's radius and to introduce curvature of the sort actually observed. However, it is clear from the diagram that in order to influence appreciably the observations the zone of instability must extend upward to optical depths less than 1. This last point might have been anticipated, since the contribution from lower depths is slight, and there would be no reason to expect any violent discontinuity in the temperature gradient where the two layers merge.

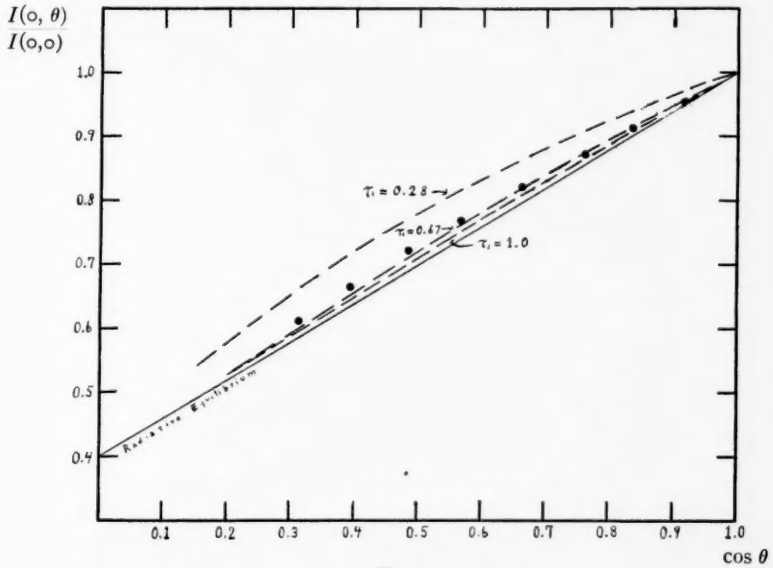

FIG. 1

On the other hand, we have seen that the predicted unstable layer is confined to greater depths (below $\tau \approx 2$). For this reason it is not possible at the present time to conclude from observations of limb darkening whether the prediction is correct. If later there develop grounds to believe that the region of instability can affect the surface layers, it will be worth while to refine our assumptions in order to predict exact temperature gradients. The general character of the curves of darkening to be expected has been established by our present investigation and is not altered greatly by even considerable changes in the constants.

It is of incidental interest to see how closely the observations could be fitted if we were permitted to choose an appropriate value of τ_1. Figure 2 shows a curve of darkening for $\tau_1 = 0.5$, for which a weighted mean value of γ within the adiabatic layer was used to improve the approximation. The computation was carried out for

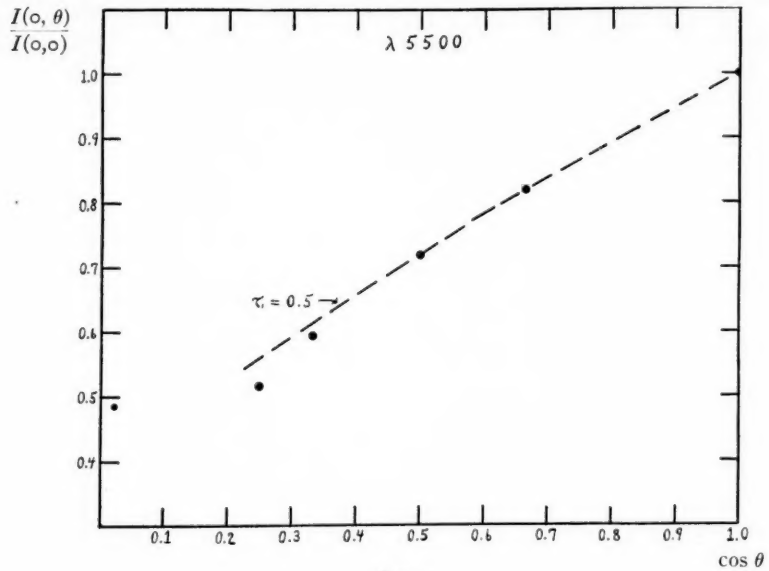

FIG. 2

λ 5500 by an approximate summation, using Plaskett's convenient tables,[3] in order to allow comparison with the measures in this spectral region by Moll, Burger, and van der Bilt, indicated by the filled circles in the diagram. The fit is close except for $\cos\theta = 0.4$, where the observations may be less certain because of atmospheric scattering and scintillation.

In conclusion I should like to acknowledge many helpful discussions of this problem with Dr. S. Chandrasekhar.

YERKES OBSERVATORY
September 1937

LINE INTENSITIES IN ULTRAVIOLET STELLAR SPECTRA

LAWRENCE H. ALLER AND LAURENCE G. STODDARD

ABSTRACT

Eye-estimates of intensity, on an arbitrary scale, of 17 ultraviolet lines of neutral iron, magnesium, and aluminum have been made on 66 plates distributed among 31 representative supergiants, giants, and dwarfs. These intensities are compared with half-breadths computed on the basis of Pannekoek's recent theory, and the results are discussed.

In a recent paper Pannekoek[1] has attempted the theoretical calculation of line intensities in stellar spectra. Starting with an assumed composition of a stellar atmosphere based on Russell's work,[2] and using formulae for the stellar absorption coefficient supplied by Menzel and Pekeris,[3] he has deduced numerical values for the coefficients of opacity and absorption. These data have been utilized in his numerical integration of the equations of radiative transfer, making possible the theoretical determination of the half-breadths of spectral lines.

The present writers have undertaken an observational test of this theory, using eye-estimates of intensity on an arbitrary scale. For this purpose a series of plates, taken by Professor C. D. Shane with the quartz spectrograph attached to the Crossley reflector of the Lick Observatory, was used. While the theory gives half-breadths and observations yield eye-estimates of intensity, certain features can be examined, such as the theoretical predictions of maxima or the complete absence of lines.

THE OBSERVATIONAL MATERIAL

The observational material consists of 172 spectrograms taken during the summer of 1926. These plates were distributed among 65 stars. Of this group, 27 stars were rejected for one of the following reasons: (1) nebulous lines or definite evidence of rotation; (2) spectroscopic binaries with two spectra visible; (3) poor plates.

[1] *Pub. Astron. Inst. Amsterdam*, **4**, 1935, and Addendum.

[2] *Ap. J.*, **70**, 11, 1929; **75**, 337, 1932; and **78**, 281, 1933. [3] *M.N.*, **96**, 77, 1936.

Under (1) a number of early-type stars were rejected which showed fuzzy lines or possessed a high rotational velocity (greater than 100 km/sec), according to the studies of Struve and Elvey and Miss

TABLE 1

Star	Spectral Class	Vis. m	Vis. M	No. of Plates
ϵ Serpentis	A6s	3.8	1.8	2
γ Virginis	F0	3.8	2.8	3
41 Cygni	cF4	4.1	−0.9	4
χ Draconis	F5	4.0	4.0	3
γ Serpentis	F5	3.9	3.3	2
α Equulei	F6	4.1	2.6	4
η Bootis	F7	2.8	3.2	2
Sun	G0	.....	4.8	4
λ Serpentis	G1	4.5	4.1	2
β Draconis	cG2	3.0	−1.7	2
37 Leo Minoris	cG2	4.8	−1.6	1
η Pegasi	G2	3.4	0.6	2
ϵ Leonis	cG3	3.1	−1.3	1
δ Bootis	G4	3.5	0.8	1
β Bootis	G4	3.6	0.3	2
μ Herculis	G4	3.4	4.2	2
ξ Bootis	G5	4.8	5.3	2
α Ursa Majoris	G6	2.0	0.0	3
σ Draconis	G9	4.8	5.6	1
ϵ Bootis	K0	2.7	−0.1	1
α Bootis	K0	0.2	0.2	4
χ Ursa Majoris	K1	3.8	0.4	2
θ Herculis	cK1	4.0	−1.3	2
70 Ophiuchi	K1	4.3	5.9	2
β Ursa Minoris	K5	2.2	−0.5	1
γ Draconis	K5	2.4	−0.1	3
61 Cygni	K6	5.6	7.7	1
β Andromedae	M0	2.4	0.2	2
α Scorpii	M1	1.2	−3.8	1
β Pegasi	M2	2.6	−0.6	2
α Herculis	M5	3.5	−1.9	2

Westgate.[4] It was necessary to select stars without appreciable rotational velocities, since this theory does not take account of rotation. Since the lists of Struve and Elvey and Miss Westgate are not complete, it was possible for us to reject only those stars which their lists

[4] *Ap. J.*, **71**, 227, 1930; **77**, 141, 1933.

had also contained. However, the stars with nebulous lines were all rejected, as this phenomenon was believed, in general, to be due to rotation. Spectroscopic binaries with two spectra visible were rejected for obvious reasons.

For some stars only one or two plates were available, and these were sometimes either underexposed or did not have excellent definition. Among the 38 remaining stars, seven were of early type and were not used in the present investigation, which deals with lines of neutral iron, magnesium, and aluminum. The hot stars usually contained too few lines of any kind. In the final study, 66 spectrograms of highest quality were used. The plates were distributed among a representative set of giants and dwarfs, with a few supergiants (see Table 1).[5]

THE SELECTION OF THE LINES STUDIED

The spectra cover the range from λ 3500 to the H and K lines. In the cooler stars the number of lines is large, and the blends are very numerous. The most prominent lines are due to iron with fainter ones of titanium, nickel, cobalt, aluminum, and magnesium. Plates of Arcturus, the sun, and χ Draconis were measured and reduced by the Hartmann formula, on the basis of the iron comparison spectrum. The *Revised Rowland Table* was used for identifying the lines. The only lines retained for purposes of comparison were either unblended or possessed one predominant component, preferably blended with a line of the same element in the same state of ionization. Table 2 gives a summary of the lines studied with the multiplet designations and Rowland intensities. Some lines beyond λ 3500 were studied; but the weakness of the continuous background vitiated the estimates, and a discussion of these lines is not included here.

ESTIMATES OF THE INTENSITIES

The good plates were divided into six classes, according to the nature of the continuous spectrum. The lines to be studied were marked on an enlargement of the spectrum of the moon. The plates of each group were thoroughly mixed, and the intensities of the chosen lines were estimated visually on a scale of 15. Estimates of the intensities of all the groups were carried out, and the procedure

[5] *Ibid.*, **81**, 187, 1935; *Mt. W. Contr.*, No. 511.

was repeated until the intensities on each plate had been estimated five times. Means were then computed.

The reason for dividing the plates into these groups and estimating the intensities for each group separately was to see if there was

TABLE 2*

Line	Ground Energy (Volts)	J	Rowland I	Multiplet
Aluminum:				
λ 3944.02.....	0.000	$\frac{1}{2}-\frac{1}{2}$	15	$3^2P^\circ-4^2S$
3961.54.....	0.014	$\frac{3}{2}-\frac{1}{2}$	20	$3^2P^\circ-4^2S$
Magnesium:				
λ 3838.50.....	2.705	2–1	25	$3^3P^\circ-3^3D$
Iron:				
λ 3820.44.....	0.855	5–4	25	$a^5F-y^5D^\circ$
3825.89.....	0.911	4–3	20	$a^5F-y^5D^\circ$
3849.98.....	1.007	1–0	10	$a^5F-y^5D^\circ$
3734.88.....	0.855	5–5	40	$a^5F-y^5F^\circ$
3749.50.....	0.911	4–4	20	$a^5F-y^5F^\circ$
3763.80.....	0.986	2–2	10	$a^5F-y^5F^\circ$
3767.21.....	1.007	1–1	8	$a^5F-y^5F^\circ$
3709.26.....	0.911	4–3	8	$a^5F-y^5F^\circ$
3719.95.....	0.000	4–5	40	$a^5D-z^5F^\circ$
3737.14.....	0.051	3–4	30	$a^5D-z^5F^\circ$
3581.21.....	0.855	5–6	30	$a^5F-z^5G^\circ$
3608.87.....	1.007	1–2	20	$a^5F-z^5G^\circ$
3631.48.....	0.954	3–4	15	$a^5F-z^5G^\circ$
3570.14.....	0.911	4–5	20	$a^5F-z^3G^\circ$

* From Miss Moore's *A Multiplet Table of Astrophysical Interest.*

any dependence of the intensity estimates on the density of the background. It was found that, when the results were plotted, there was not much difference, except at the ends of the spectral range, for plates of the extreme groups. The plates were all Eastman 40's, except for one Eastman 33.

THE THEORETICAL CALCULATION OF THE INTENSITIES ON THE BASIS OF THE PANNEKOEK THEORY

If we confine our attention to lines sufficiently strong, so that the point at which the intensity falls to half that of the continuous background is within the resonance wings and not within the Doppler core, we may use Pannekoek's abbreviated formula

$$(\Delta\lambda)^2 \propto \left(\frac{\lambda}{4000}\right)^2 \frac{\delta}{\gamma} \frac{Axyf}{s},$$

where δ/γ is the ratio of the quantum mechanical to the classical half-breadth of the scattering coefficient, f is the oscillator strength related to the Einstein probability coefficient, A is the abundance, x is the percentage in the proper state of ionization, y is the percentage excited to the ground state of the transition in question, and s is the appropriate scattering coefficient. In practice we compare the same line throughout the spectral range. Thus $\lambda/4000$, δ/γ, and f are constant and A is assumed constant, so that for a given line we may put (for two stars of temperatures, T_1 and T_7)

$$\frac{(\Delta\lambda)^2_{T_1}}{(\Delta\lambda)^2_{T_2}} = \frac{x_1 y_1 s_2}{x_2 y_2 s_1}.$$

The percentage of atoms in a given state of excitation and ionization was computed by means of the Saha and Boltzmann expressions. The partition functions were computed with the aid of the data of Bacher and Goudsmit. Modifications of the Boltzmann formula for deviations from thermodynamic equilibrium were not considered. The effect of the dilution of the radiation upon the ionization was taken into account.

Pannekoek considers the problem of line formation under the following three conditions:

Case A.—The number of atoms is decreasing, owing to ionization, as the temperature increases (the case of neutral atoms in the hotter stars).

Case B.—The number of atoms is constant or a maximum (e.g., the case of neutral atoms of metals such as *Fe*, *Cr*, *Ni*, etc., at low temperatures, or of *Ca* before the second ionization sets in but when the neutral calcium is all ionized).

Case C.—The number of atoms is increasing, owing to ionization. This case is of significance only for the ionized atoms (see Fig. 1).

Now s is the value of the scattering coefficient for a point in the line for which the intensity falls to one-half that of the continuous spectrum. When all the atoms are in the proper state of ionization, s is equal to s_0. We may write for Case A,

$$s = s_0 \frac{P}{P + K},$$

by virtue of the well-known ionization formula $(xP/[1 - x]) = K$. The electron pressure P is much smaller than K for the case of high ionization, so that for the purposes of his numerical integrations Pannekoek took $s = (s_0P)/K = \sigma P$, where $\sigma = s_0/K$. For Case B he merely took s as constant. In the present investigation we need concern ourselves only with Cases A and B, since we are dealing with lines of neutral atoms which remain approximately constant in

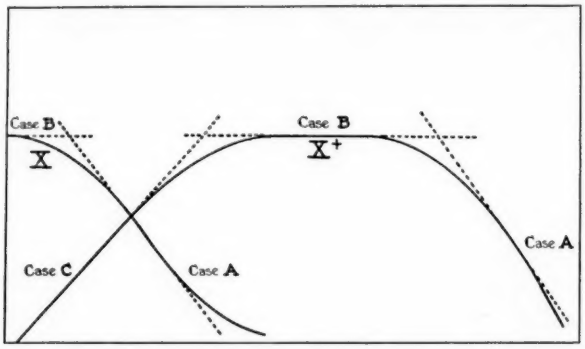

FIG. 1.—Pannekoek's three cases for a hypothetical element X and X^+, e.g., Mg and Mg^+.

number over a certain temperature range and then decrease for higher temperatures.

Pannekoek tabulates σ and s with the surface gravity g, $5040/T$, and the wave length as arguments. Now in Case A, s_0 was taken as equal to σK in the numerical integrations. Actually, we should have had $(K + P)$ instead of K, so that, after having computed K and y and after having taken σ and P from the tables, we have

$$(\Delta\lambda)^2 \propto \frac{y}{\sigma(K + P)} .$$

For the Case B we look up s in Pannekoek's Table 29*a*, and, noting that $s = (s_0P)/(P + K)$,

$$(\Delta\lambda)^2 \propto \frac{y}{s}\frac{P}{P + K} .$$

For the purposes of the numerical integrations, the neglect of these proper factors was justifiable; but in comparing a line from star to

star where the surface gravity and temperature vary (and hence K and P must vary), we must include them, to get the best results. Usually, the intensity of a line was computed on the basis of both cases, A and B, for those intervening regions in which neither case is strictly valid.

We need to know the surface gravity and temperature for each spectral class among the stars studied. The surface gravity and temperature are connected by the empirical formulae given by Russell:[6]

$$\log_{10} \frac{g}{g_0} = -0.65 + 0.28z \qquad \text{(giant sequence)},$$

$$\log_{10} \frac{g}{g_0} = +0.76 - 0.97z \qquad \text{(main sequence)}.$$

For the sun, $\log g_0$ is 4.4; $z = 11{,}600/T$.

The temperature scale adopted was that given in Russell, Dugan, and Stewart's *Astronomy*.[7] For use in the ionization formula $1 - x = P/(P + K)$, the mean electron pressures, P_m, are taken from Pannekoek's Table 22, and K is computed in the usual manner. The σ and s are found by interpolation in Tables 28 and 29. For the supergiant stars no temperature scale was available, and we have assumed the following values by the extrapolation of the difference between giants and dwarfs for the temperature of a given spectral class:

Fo	F5	Go	G5	Ko	K5	M2	M5
7400	6500	5500	4200	3700	3200	3000	2600

On this basis the absolute bolometric magnitudes for the stars used were computed from the expression

$$M_v - M_r = 10 \log T + \frac{29{,}500}{T} - 42.1,$$

given by Russell, Dugan, and Stewart. Use was then made of a table published by Mrs. Payne-Gaposchkin in her *Stars of High*

[6] *Ap. J.*, **78**, 270, 1933; *Mt. W. Contr.*, No. 477, 1932.

[7] P. 753.

Luminosity,[8] to find appropriate surface gravities for the supergiant stars. We adopt the following:

Temperature....	7200	6300	5600	5040	4200	3600	3150	2520
log g.....	3.0	2.7	2.5	2.2	1.8	1.3	1.1	1.0

COMPARISON OF THEORY AND OBSERVATION

The eye-estimates of intensity were plotted against temperature for each line in the dwarf, giant, and supergiant sequences. The best line through the points was drawn in each case. Sometimes the scatter was bad, but for the most part the observations permitted fairly definitive curves to be drawn. Typical curves are reproduced in Figure 2.

The logarithms of the half-breadths, as computed by the method outlined above, were plotted against the temperature. For purposes of further comparison between theory and observation, the actual half-breadths were plotted also. A comparison of our scale with the Rowland scale was also made by use of the plates for the sun. In regard to the scatter of the individual values of the intensity estimates, it should be remarked that not all of the scatter is due to errors of observation. Some of it may certainly be attributed to peculiarities of the individual stars, which, for a given spectral class, often showed considerable range in absolute magnitude.

Aluminum.—The only aluminum lines available were λ 3944 and λ 3961. Theory predicts that above 5000° the lines should be slightly stronger in dwarfs and giants than in supergiants, but that below 5000° the lines should be strongest for the supergiants with a maximum half-breadth of about three times that of the dwarfs. Flat maxima are predicted at 4000° for the dwarfs and near 3000° for the giants and supergiants.

Actually the lines appear at a higher temperature in the dwarfs and reach a greater maximum intensity than in either the giants or the c stars. The maximum is poorly defined in all cases. The lines are strongest for the dwarfs, next strongest for the giants, and weakest for the supergiants. The mean maximum intensity is 4.5 for the c stars and 8 for the dwarfs, on our scale.

[8] P. 113.

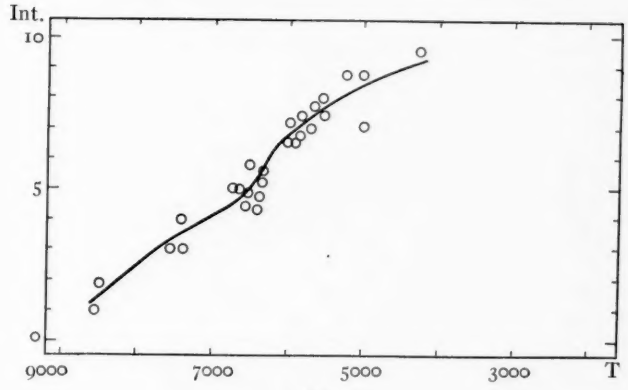

FIG. 2a

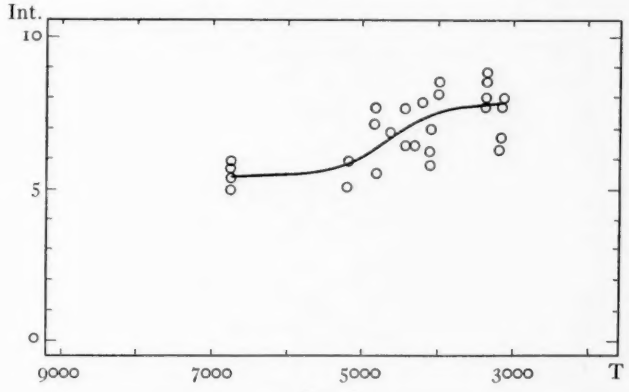

FIG. 2b

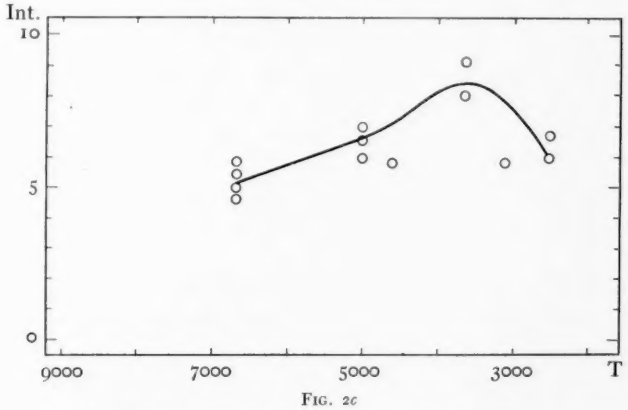

FIG. 2c

FIG. 2.—Observed intensity of λ 3631, *Fe* and Cr^+; (*a*) dwarf, (*b*) giant, (*c*) super giant. The temperature is in degrees absolute.

Magnesium.—For magnesium, λ 3838, theory predicts lines of about equal intensity in giants, supergiants, and dwarfs, down to about 5000°. Below 5000° the line should be strongest in giants and supergiants and weakest in the dwarfs. (At 4200° the line should be

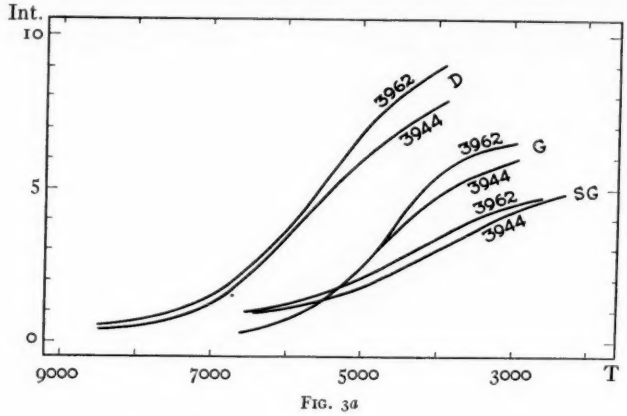

FIG. 3a

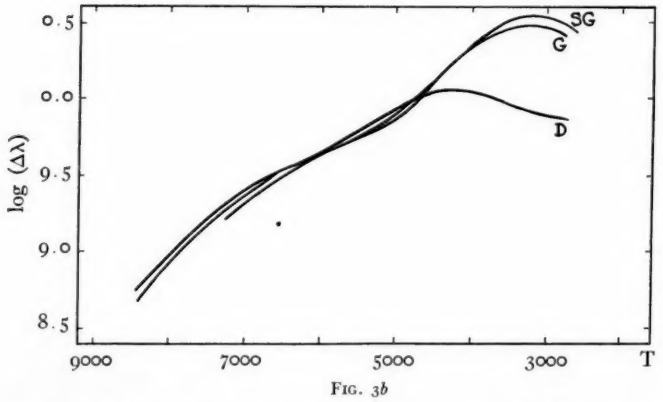

FIG. 3b

FIG. 3.—The intensities of the aluminum lines λ 3944 and λ 3962 in dwarfs, giants, and supergiants; (*a*) observed and (*b*) theoretical curves.

twice as strong in the supergiants as in the dwarfs.) The predicted maxima for the supergiants, giants, and dwarfs are, roughly, at 4000°, 4100°, and 5000°, respectively.

The observational data are rather uncertain, but they definitely show that the line appears at a higher temperature in the dwarfs,

and for the higher temperatures is much stronger in these stars than in the giants and supergiants. The maximum intensities appear to be about equal for dwarfs and supergiants; but the maximum for the giants seems slightly weaker, probably the effect of observational

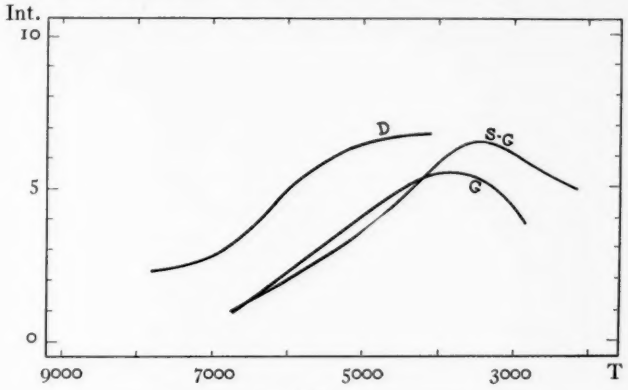

FIG. 4a

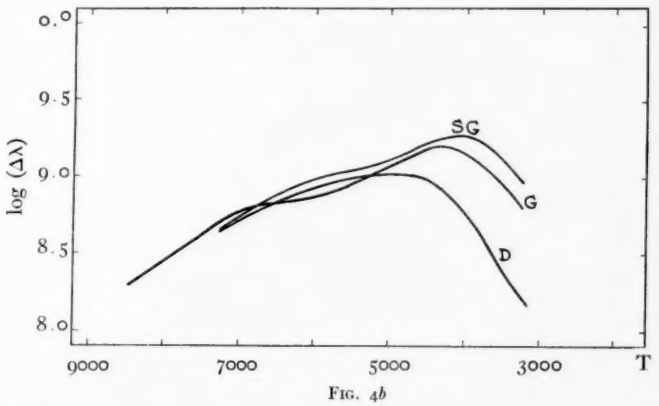

FIG. 4b

FIG. 4.—The intensities of the magnesium line λ 3838; (*a*) observed and (*b*) theoretical.

errors. The maxima for giants and supergiants appear at 4000° and 3500°, respectively; and the maximum for the dwarfs is not indicated.

Iron.—For iron, the material is the most extensive and we may draw the soundest conclusions. For all the lines except those beyond

the Balmer limit, the theory predicts roughly equal intensities for giants, supergiants, and dwarfs for any temperature above 5000°. For the $a^5F - z^5G$ multiplet the lines should be strongest for the dwarfs at the higher temperatures, but in all three cases the intensity

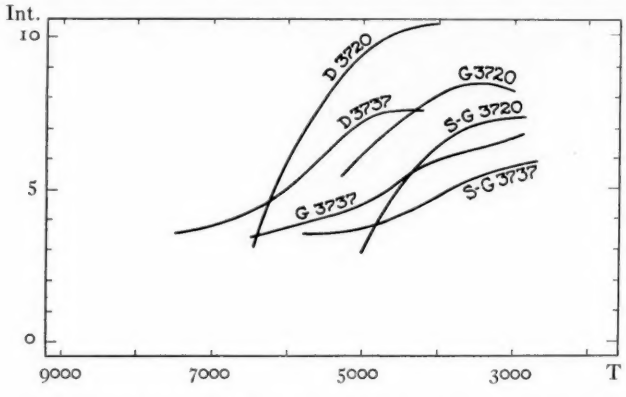

FIG. 5*a*.—Observed intensities of the iron lines λ 3720 and λ 3737 in dwarfs, giants, and supergiants.

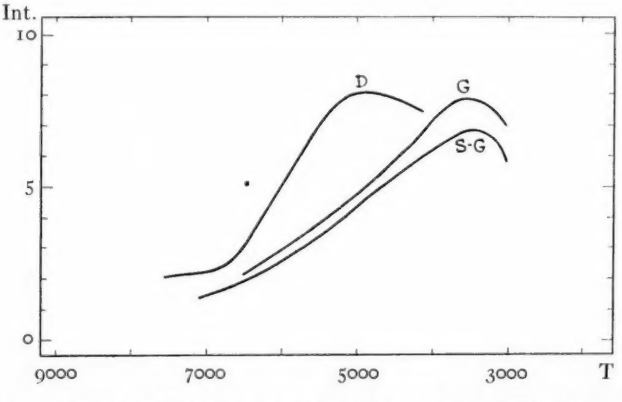

FIG. 5*b*.—Observed intensities of the iron line λ 3826 in dwarfs, giants, and supergiants.

should fall rapidly as the temperature increases. The theory predicts strong maxima for the supergiants with half-breadths ranging from three to five times those of the same line in the dwarfs. For the lines for which the excitation potential is of the order of 1 volt, the temperatures of the maxima are, respectively, 3600°, 3900°, and 4700°, for the

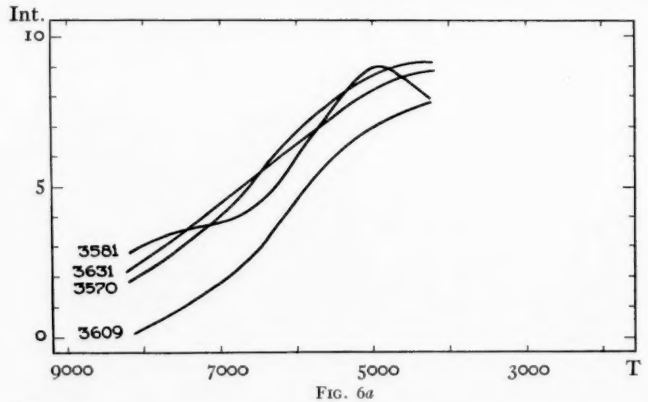

FIG. 6a

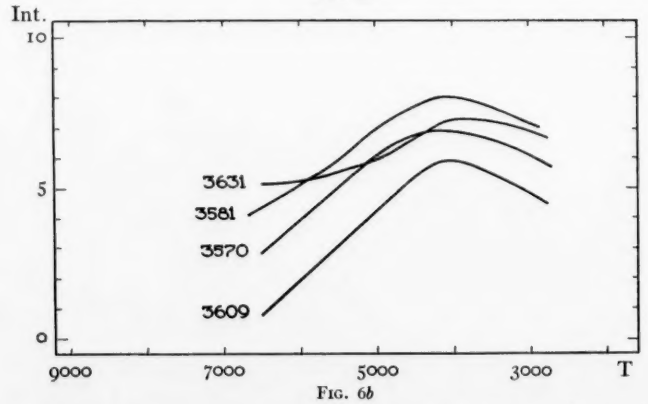

FIG. 6b

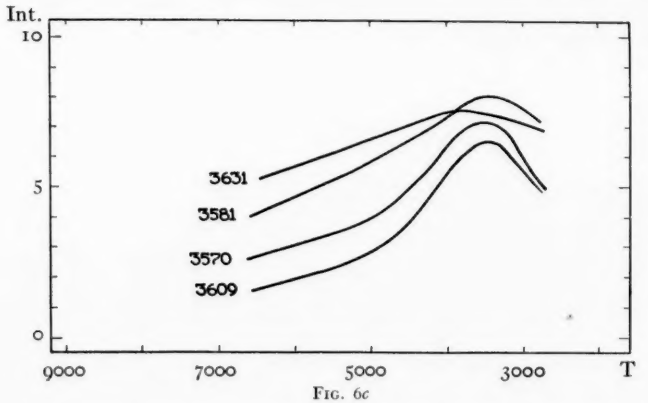

FIG. 6c

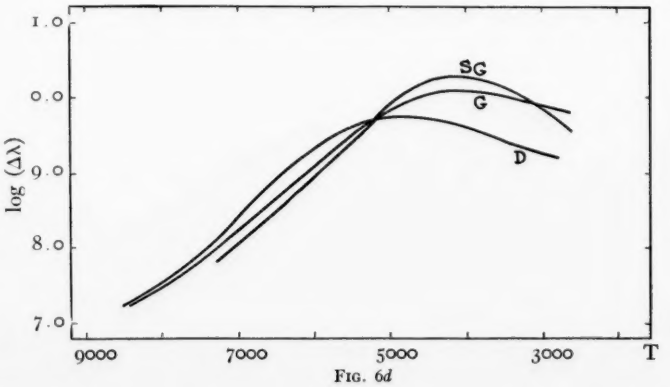

FIG. 6d

FIG. 6.—Observed and theoretical curves for the *Fe* lines λλ 3631, 3581, 3570, and 3609. At the higher temperatures λ 3631.5 is blended with λ 3631.7 of Cr^{+}; (*a*) dwarfs, (*b*) giants, (*c*) supergiants, and (*d*) theoretical.

supergiants, giants, and dwarfs. For the lines whose ground level is about 0 volts, the maxima are at 3500°, 3600°, and 4200°.

In all cases the dwarf lines are much stronger than the giant and supergiant lines for the higher temperatures, and the giant lines are usually more intense than the supergiant lines. The maximum intensities of the lines are certainly just as great for the dwarfs as for the supergiants, and probably greater. The $a^5D - z^5F$ multiplet yields a very uncertain maximum; but for the other multiplets of iron studied, the positions of the maxima seem to be nearly the same as that predicted by theory for the supergiants. The agreement is generally good for the giants; the single discrepancy is probably due to errors of observation. For the dwarfs the maxima are near the end of the range of temperature to which the observations extend, and therefore the agreement between theory and observation cannot be tested.

A bad discrepancy between theory and observation exists at the head of the Balmer series. Theory predicts that the lines of the $a^5F - z^5G^o$ and $a^5F - z^3G^o$ multiplets, λλ 3581, 3570, 3609, and 3631,[9] should disappear near 7400°; but they persist to 8400° along the main sequence. Data for the giants are not available for the higher temperatures, but the lines are still strong for the hottest star in the list. This contradiction between theory and observation also holds for the supergiants.

To summarize our results, we may say that the theory tends to predict too intense lines for the giants and supergiants, as compared with the dwarfs, especially at the higher temperatures. Excluding the case of magnesium, for which the data are rather weak, the maxima, as predicted by theory, agree quite well with the observations. A notable discrepancy between theory and observation seems to occur for the lines below the Balmer limit. These lines should fall off in intensity very rapidly where hydrogen begins to be appreciably ionized, but they persist to much higher temperatures than one would expect on the basis of the theory. The discrepancy seems to be real, and it is not possible to account for it on the basis of blends.

[9] At higher temperatures, λ 3631.5 *Fe* is blended with λ 3631.7 Cr^+, $a^4P - z^4P^o$.

We are indebted to Professor Shane, who suggested the problem and furnished the observational material and under whose guidance the investigation was carried out. We are also thankful to Mr. James Fidiam, of San Francisco, for his beautiful enlargements of many of our plates and to Mr. Gordon Wares, of the Yerkes Observatory, who helped in classifying the plates.

UNIVERSITY OF CALIFORNIA
July 17, 1937

THE FUNDAMENTAL ARC SERIES IN SODIUM AND ITS PRESENCE IN THE SUN

PAUL ROOD AND R. A. SAWYER

ABSTRACT

Using a powerful discharge tube of new design, the infrared arc spectrum of sodium has been photographed, and measured with a thermopile, as far as λ 12679, $3^2D-5^2F^\circ$. In addition to this line, five new members of the $^2D^2F^\circ$ series in *Na* I were measured with an accuracy of ±0.2 or ±0.3 A. Data supplied by Miss C. E. Moore and Mr. H. D. Babcock, of the Mount Wilson Observatory, indicate that this sodium series is present in the solar spectrum. New values for the $^2F^\circ$ terms are given. In addition, three members of the $4^2S-5^2P^\circ$ series were observed for the first time.

In connection with their program of identification of the infrared solar lines at the Mount Wilson Observatory, Miss Charlotte E. Moore and Mr. H. D. Babcock have called to our attention the fact that no recent or accurate measures are available of the Bergmann series in the arc spectrum of sodium. The approximate positions of the lines can be predicted within a few angstroms, but no values good enough for certain identification are known.

The first measurement in the sodium $^2D^2F^\circ$ series was made in 1907 by Bergmann,[1] who in his original work observed, but did not classify, the second member of the series. In the next year, both the first and second members were measured by Paschen,[2] who gave their wave lengths as λ 18459.42 ± 2. and λ 12677.54 ± 8. No other measurements in the fundamental series appear to have been made, although a calculated 6^2F° term has been obtained from a supposed $3^2P^\circ - 6^2F^\circ$ combination at λ 4665 and λ 4660. This term does not agree well with the one determined in the present work.

The successful measurement of the lines of the fundamental series requires a vacuum source, since in open arcs they appear broad and fuzzy, if they appear at all. The source finally found most suitable was the positive column in a large end-on discharge tube. The tube was of pyrex glass, 3 cm. in diameter and about a meter long, with large cylindrical aluminum electrodes in side arms. Pure redistilled sodium was introduced into the tube in glass boats, and the re-

[1] *Zs. f. Wiss. Phot.*, **6**, 113 and 145, 1908. [2] *Ann. d. Phys.*, **27**, 543, 1908.

quired pressure of sodium vapor was produced by an electric furnace surrounding the tube. The discharge was carried by pure helium or neon. The series was more intense in helium; but the third and fifth members fell too close to helium lines for measurement, and a discharge in helium-free neon was used to obtain these lines. The helium or neon was circulated through charcoal traps in liquid air and through the tube by means of a glass mercury pump. Sixty-cycle current from a 2000-volt transformer at currents of 1 to 1.5 amperes, at suitable pressures of sodium and of the gas used, provided a very intense sodium light.

The intensity of the sodium spectrum in the discharge was sufficient to permit thermopile measurements in the infrared with a grating spectrograph. This instrument,[3] which was placed at our

TABLE 1

MEASUREMENT OF THE $3^2P^0-4^2S$ DOUBLET OF SODIUM

Classification	Wave Length Observed	ν	$\Delta\nu$ Observed	$\Delta\nu$ Calculated	Error
$3^2P^0-4^2S$	11403.2	8767.1	.....	.....	.....
$3^2P^0-4^2S$	11381.0	8784.2	17.1	17.2	0.1

disposal by Professor E. F. Barker, who assisted in its use, has mirrors of 100 cm focal length and a 1100 lines per centimeter grating. Using the helium line λ 10830.3 as a standard, the second member of the sodium fundamental series, $3^2D - 5^2F^0$, was measured as λ 12679.0 $\pm$ 0.5 A. The contour of this line was mapped, and its width was found to be not greater than the slit width of the spectrograph, an indication of the sharpness of the lines from this discharge. As a test of the accuracy of this measurement, the $3^2P^0 - 4^2S$ doublet, whose separation can be calculated from known terms, was measured, with the results shown in Table 1.

The shorter members of the fundamental series were photographed with a Littrow-type flint-glass spectrograph having a dispersion, at 10,000 A, of about 70 A per millimeter. Eastman M, Q, and Z plates were used in the regions of their respective optimum sensitivities. The exposures ran from $3\frac{1}{2}$ to 5 hours. The helium

[3] Barker and Meyer, *Trans. Faraday Soc.*, **25**, 912, 1929.

or neon lines emitted by the discharge tube, depending on the gas used, were taken as standards, the values being those from the recent measurements at the Bureau of Standards.[4] For converting the wave lengths to wave numbers, the values for the dispersion of air by Meggers and Peters,[5] extrapolated above λ 10,000, were used.

The final values adopted for the fundamental series lines of sodium are given in Table 2. The $^2F^0$ term values and effective quantum numbers are also given.

TABLE 2

THE FUNDAMENTAL SERIES OF SODIUM, $3^2D - m^2F^0$
$3^2D = 12276.18$

Term	Wave Length	Wave Number	m^2F^0	N_{eff}
4^2F^0*	18459.5	5415.8	6860.4	3.9994
5^2F^0	12679.0	7884.8	4391.4	4.9989
6^2F^0	10834.4	9227.3	3048.9	5.9993
7^2F^0	9961.0	10036.4	2239.8	6.9995
8^2F^0†	9466.0	10561.2	1715.0	7.9991
9^2F^0	9154.7	10920.4	1355.8	8.9965
10^2F^0	8943.6	11178.1	1098.1	9.9966
11^2F^0	8796.	11366.	910.	10.981

* Paschen's value, not measured in the present work.
† Calculated term. Interference in both helium and neon.

With the exception of λ 8796, which appeared on only one plate, the lines were each measured on two to four plates. The consistency of the various values indicated a reliability of ±0.2 or ±0.3 A for these lines. A further direct check on the accuracy was given by measurements on three members of the $4^2S - m^2P^0$ series, whose wave lengths can be computed from their known terms, determined from very accurate measurements at shorter wave lengths. These lines were here observed for the first time. The comparison is given in Table 3.

Miss Moore and Mr. Babcock have supplied us with information

[4] Meggers and Dieke, *Nat. Bur. Stand. J. Res.*, **9**, 121, 1932, Meggers and Humphreys, *ibid.*, **10**, 427, 1933.

[5] *Bull. Bur. Stand.*, **14**, 698, 1919. See also Babcock (*Phys. Rev.*, **46**, 382, 1934) on a method for obtaining infrared wave numbers from Kayser's *Tabelle der Schwingungszahlen.*

on the closest solar line to each measured sodium line of the fundamental series and also its probable solar identification. This information is given in Table 4. It is evident that this sodium series appears in the solar spectrum.

TABLE 3

NEW LINES IN $4^2S-m^2P^o$ SERIES OF SODIUM

Classification	Observed	Calculated*	Error
$4^2S-5^2P^o$.....	10747.2	10747.3	0.1
$4^2S-6^2P^o$.....	8649.6	8650.0	.4
$4^2S-7^2P^o$.....	7809.4	7809.6	0.2

* The calculated value is the mean wave length of the doublet.

TABLE 4

THE FUNDAMENTAL SERIES OF SODIUM IN THE SUN

Term	Laboratory	Sun			
	Wave Length	Nearest Solar λ	Int.*	Solar λ *minus* Lab. λ	Solar Ident.
4^2F^o†.....	18459.5	Too far out			
5^2F^o.....	12679.0	80.40	6*N*	+1.4	*Na*
6^2F^o.....	10834.4	34.01	5	−0.4	*Na*
7^2F^o.....	9961.0	61.38	0	+0.4	*Na*
8^2F^o‡.....	9466.0	65.98	−3?	−0.0	*Na*
9^2F^o.....	9154.7	54.122	−1*N*	−0.6	Atm. / Atm. *Na?*
		55.4	7		
10^2F^o.....	8943.6	43.058	1	−0.5	*Fe*
11^2F^o.....	8796.	96.491	1	+0.5	*Fe*

* Underline denotes that estimated intensity is from more than one plate.

† Paschen value of wave length.

‡ Wave length calculated.

We are much indebted to Dr. H. G. Beutler for aid in the distillation of the sodium and in the design of the tube, to Professor E. F. Barker for his co-operation in the infrared grating measurements, and to Miss C. E. Moore and Mr. H. D. Babcock, who instigated this work and supplied the solar data.

DEPARTMENT OF PHYSICS
UNIVERSITY OF MICHIGAN
October 1937

NOTES

THE ORBIT OF b PERSEI

ABSTRACT

A new orbit determination of b Persei confirms Harper's orbit and supports his view that changes are taking place in some of the elements.

Previous orbit determinations of b Persei ($\alpha[1900] = 4^h10^m.7$, $\delta[1900] = 50°03'$, visual magnitude 4.57, type A2) have been made by Cannon[1] from Ottawa observations of 1910–1911 and by Harper[2]

TABLE 1

Date (G.C.T.)	Phase	Velocity (Km/Sec)	O−C (Final)
1934 Sept. 26.306....	0.000	− 9.2	+3.8
28.354....	0.521	+58.6	−4.2
Oct. 2.405....	1.517	−10.7	+3.5
7.358....	0.360	+55.9	+6.7
8.412....	1.414	−23.0	−0.8
13.372....	0.265	+32.5	−1.1
22.297....	0.026	−10.4	−0.7
30.401....	0.493	+63.9	+2.2
Nov. 1.378....	0.942	+14.8	−7.4
7.415....	0.870	+41.9	+8.3
24.432....	1.086	− 1.8	−1.5
Dec. 7.256....	0.163	+12.7	−1.1
11.307....	1.159	− 8.7	+0.8
1935 Jan. 5.354....	0.241	+29.2	+0.1
5.394....	0.281	+36.8	+0.3
14.385....	0.108	+ 2.2	−1.4
14.410....	0.133	+ 0.6	−7.6
22.076....	0.162	+17.1	+3.3
26.990....	0.494	+58.4	−3.3

from Victoria observations of 1929–1930. Harper's orbit differed from Cannon's in such a way as to indicate real changes in some of the elements.

The material for the present orbit determination consisted of a series of 19 spectrograms made with the Bruce single-prism spectro-

[1] *Pub. Dom. Obs. Ottawa*, **1**, 283, 1914.

[2] *Pub. Dom. Ap. Obs. Victoria*, **4**, 309, 1930.

graph attached to the Yerkes 40-inch telescope, the series extending from September 26, 1934, to January 26, 1935. On these spectrograms the lines measured were λλ 3933.27, 4101.74, 4340.47, 4481.23, and 4549.53.

The period adopted by Harper, 1.52738 days, fitted the observations better than any other; accordingly, it was used. The data for the individual observations are shown in Table 1.

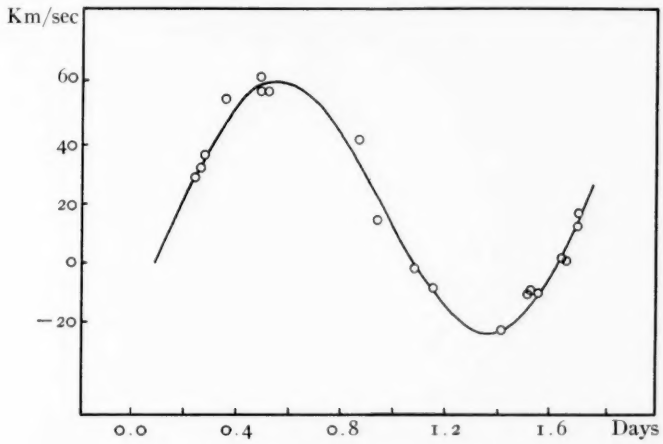

FIG. 1.—Velocity-curve of b Persei

Four observations were put into two groups, resulting in 17 normal places. Preliminary elements were chosen, using a graphical method by R. K. Young. They are as follows:

$P = 1.52738$ days	$K = 43.5$ km/sec
$e = 0.05$	$\gamma = +20.6$ km/sec
$\omega = 270°$	$T =$ JD 2418956.643

Since the value of e was so small, T was fixed and a least-squares solution was carried out for corrections to e, ω, K, and γ, resulting in small corrections to the preliminary elements. The final elements, together with the computed probable errors, are shown in Table 2, along with Cannon's and Harper's elements for comparison. The probable error of a single observation is: for Cannon's observations, ± 3.9; for Harper's, ± 2.4; and for the writer's, ± 2.8.

Harper has pointed out that the changes in γ and K between 1910–1911 and 1929–1930 are probably real. The 1934–1935 orbit

indicates the probability of further real changes in γ and K since 1930. The change in K is 4.2 km/sec; the change in γ is 6.3 km/sec; but, applying the corrections suggested by Moore[3] to the Victoria and Yerkes velocities, the change in γ is reduced to 4.3 km/sec. These changes are well in excess of the probable errors and are prob-

TABLE 2

Element	Cannon (1910–1911)	Harper (1929–1930)	Yerkes (1934–1935)
P	1.52732 days	1.52738 days	1.52738 days
e	0.22	0.017	0.047 ± 0.030
ω	151°.75	271°.53	$270°.95 \pm 1°.30$
γ	+23.09 km/sec	+13.53 km/sec	$+19.83 \pm 0.86$ km/sec
K	41.89 km/sec	38.85 km/sec	43.10 ± 1.37 km/sec
T	JD 2418956.166	JD 8956.662	JD 8956.643
$a \sin i$	837,600 km	815,840 km	805,440 km

ably real. No real changes are indicated in the other elements since 1930. The period of 1.52738 days connects the 1929–1930 and the 1934–1935 observations as well as could be expected in view of the changes in γ and K.

Although Cannon measured a second spectrum, neither Harper nor the writer found any evidence of it on the Victoria and Yerkes plates, respectively.

The writer wishes to express his thanks to Dr. Otto Struve for suggesting this orbit determination, the measures for which the writer made at the Yerkes Observatory in 1935 during the tenure of an 1851 Exhibition Scholarship.

J. F. HEARD

DAVID DUNLAP OBSERVATORY
September 1937

NOTE ON THE GLOBULAR CORONA

The two accompanying eclipse photographs were made at Moro, Peru (long. +78°10′.5; lat. −9°8′.5; elevation 2400 ft.), on June 8, 1937. The first (*a*), here reduced in size, was made with a 5.5-inch visual objective 72 inches in focal length, belonging to Swarthmore College. It represents an 8-second exposure in a scheduled series

[3] *Pub. Lick Obs.*, **18**, xii, 1932.

PLATE I

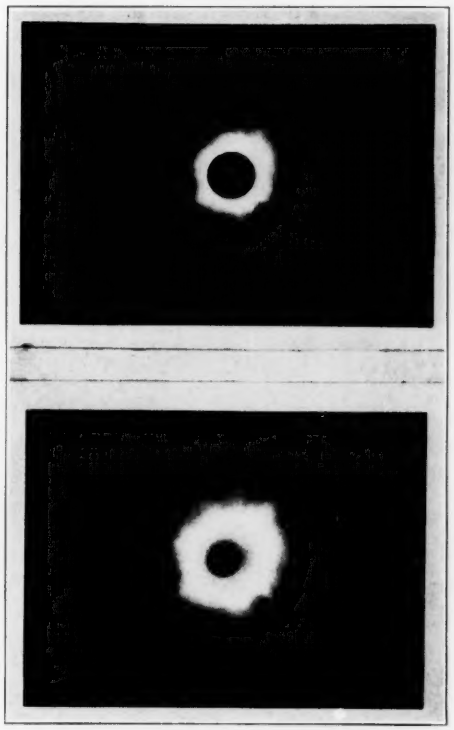

THE SOLAR CORONA OF JUNE 8, 1937
(*a*) Exposure, 8 sec., *f*/13; (*b*) exposure, 2 sec., *f*/3.5

UNIV. OF MICH.

made on Eastman 1G plates with the aid of a clock-driven polar axis.

The second photograph (*b*), enlarged to the same scale, was made with a Retina camera equipped with a lens 5 cm in focal length and operating at f/3.5. This picture, one of two made with the Retina (mounted on the same polar axis), was exposed 2 seconds, the other 4 seconds. Both the Retina pictures were made on Eastman daylight Kodachrome and were processed in the usual manner at Rochester.

Picture (*b*) shows several things. (1) The extent of the halation around the moon's disk is apparent when the two pictures (*a*) and (*b*) are compared. The disk of the moon is a dull gray, best described as mouse-colored. (2) Picture (*b*) shows the outer corona ordinarily photographed. On the original color-slide this is badly overexposed but is pale cream yellow, almost colorless. (3) This picture shows the globular corona inclosing the irregular outer corona.

This is a more adequately exposed photograph of the globular corona noted first by Major A. W. Stevens in some of his aerial photographs of the same eclipse made at an elevation of 25,000 feet off the coast of Peru. The reality of this globular envelope was tested on Stevens' films at the University of Rochester's Institute of Optics and in the Eastman Research Laboratories, where it was definitely shown not to have been introduced by the apparatus.[1] On the color-slide this ring stands out clearly as a faint sand-colored disk contrasting sharply with the greenish blue of the sky immediately surrounding the sun. The diameter of the globular corona on the original slide is about 2°.5. The 4-second exposure, too difficult to reproduce, shows a nearly identical halation-reduced lunar disk and an outer corona of the same extent, but shows the globular corona as a fainter disk 4° in diameter standing out less sharply against a lighter sky. Beneath the sun in this picture the globular corona is merged with the fainter extensions of the salmon-colored light around the horizon a few degrees away. The apparent color difference between the globular corona and the surrounding sky would seem to be of value in obtaining further observations.

A photograph showing the globular corona was obtained by

[1] Personal communication.

Putilin at the Siberian eclipse of June 19, 1936.[2] Doubtless other photographs exist of this hitherto unnoticed globular corona from earlier eclipses. An investigation of old plates might add considerably to the meager information now at hand. Planned study of this corona is a possibility for the next useful eclipse, in 1940.

The two color pictures and the series with the Swarthmore lens were made by me, as the representative of the Junior Astronomy Club of the American Museum of Natural History, on the Hayden Planetarium–Grace Eclipse Expedition.

DANA K. BAILEY

STEWARD OBSERVATORY
TUCSON, ARIZONA
September 1, 1937

PHOTOELECTRIC MEASURES OF HD 199140

The probability of a variation in the light of HD 199140 was suggested in a paper read by Dr. R. M. Petrie at the fifty-eighth meeting of the American Astronomical Society. The period deduced by Dr. Petrie from variations in the spectrum was 0.20103 day.

This star was first observed with the photoelectric photometer of the Washburn Observatory on September 25, 1937, and the variation was immediately detected. Observations were made on ten nights, from September 25 to November 10. The comparison star was HD 198820. The positions are as follows:

Star	R.A. (1900)	Dec. (1900)	Mag.	Spec.
199140.....	20^h50^m1	$+28°\ 8'$	6.44	B1s
198820.....	20 47.9	$+32\ 28$	6.30	B5sk

The light-curve is given in Figure 1; 111 observations were combined to give 22 normals. The total variation is 0.180 mag. The phase, in decimals of a period, is computed from the maximum by means of the elements

$$\text{Max.} = \text{JD } 2428802.6689 + 0^d20103 \cdot E$$
$$\text{Max.} - \text{Min.} = 0^d1235\,.$$

[2] *Ap. J.*, **85**, 341, 1937.

The short interval of the observations does not permit a correction of the period. The normal magnitudes are given in Table 1. The rise from minimum to maximum is slower than the fall from maxi-

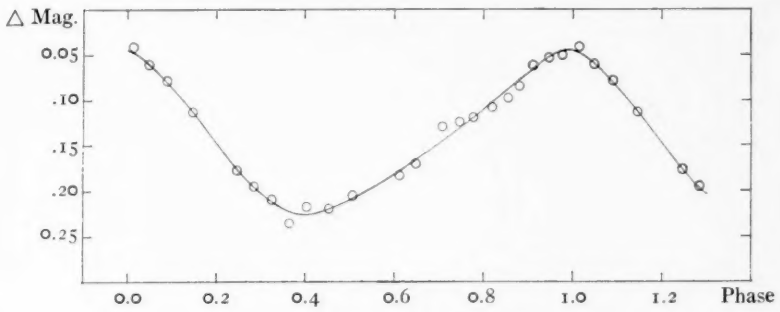

FIG. 1.—Normal magnitudes of HD 199140

TABLE 1

NORMAL MAGNITUDES OF HD 199140

Phase	Δ Mag.	Residual	Phase	Δ Mag.	Residual
$0^{p}.011$	$0^{m}.041$	−0.005	$0^{p}.611$	$0^{m}.183$	+0.004
.047	.060	.000	.648	.170	+ .005
.090	.078	− .002	.707	.129	− .016
.145	.113	.000	.746	.124	− .006
.246	.177	− .001	.778	.119	.000
.284	.195	.000	.819	.107	+ .004
.327	.209	− .002	.854	.097	+ .009
.366	.235	+ .013	.880	.084	+ .007
.402	.217	− .008	.910	.061	− .004
.453	.219	.000	.945	.053	− .001
0.507	0.205	−0.003	0.978	0.050	+0.004

mum to minimum, the former requiring 0.614 and the latter 0.386 of the entire period. This star belongs to the β Cephei class of variables but does not appear, from this short series of observations, to show any certain variation of amplitude.

C. M. HUFFER

WASHBURN OBSERVATORY
UNIVERSITY OF WISCONSIN
November 1937

NINE WHITE STARS OF LARGE PROPER MOTION

The following nine stars with spectral types earlier than F5 have been found among some 160 objects with proper motions larger than 0″.3. The complete data for these objects will be given at a future occasion, when more stars will have been observed. The magnitudes were determined by Mr. Seyfert, the spectral types by Mr. Kuiper. The last column contains the linear velocity perpendicularly to the line of sight, computed from the angular proper motion and the parallax derived from the spectral type under the assumption that

DM	R.A.	Dec.	m_{pg}	m_{pv}	Spec.	μ	V_t
							km/sec
+71° 31	0^h37^m2	+71°37′	10.30	10.34	A5sp	0″.36	820
+72 94	1:38.9	+72 58	10.16	10.17	A5sp	.33	700
+24 1005	5:47.1	+24 16	10.20	10.00	Fo	.61	830
+67 910	15:38.3	+67 08	10.46	10.46	F3	.39	520
+42 2667	15:59.9	+42 32	10.18	9.94	F2	.54	630
+13 3683	18:28.7	+13 03	11.00	10.63	A8s	.33	690
− 0 3676	19:08.2	− 0 45	9.31	9.01	F4	.53	190
+42 3607	20:05.6	+42 34	10.35	9.96	F3	.30	320
+17 4708	22:06.7	+17 36	10.00	9.27	F1	0.54	490

the star lies on the main sequence. If the directions of these motions are also considered, it is found that +72°94 would escape from the galaxy if it were a main-sequence star.[1] The other stars can, on the basis of the transverse motions alone, not definitely be said to be underluminous.

On the basis of the spectral features +71°31 and +72°94 are definitely intermediate white dwarfs, whereas +13°3683 and +24°1005 may be intermediate white dwarfs. The remaining stars are probably normal stars of high velocity.

G. P. KUIPER
C. K. SEYFERT

YERKES AND MCDONALD OBSERVATORIES

[1] Cf. *Pub. A.S.P.*, **47**, 280, 1935. The right ascension for the intermediate white dwarf +54°2461, given there, should be 20^h58^m, not 21^h58^m.

UNIV. OF MICH.

PLATE II

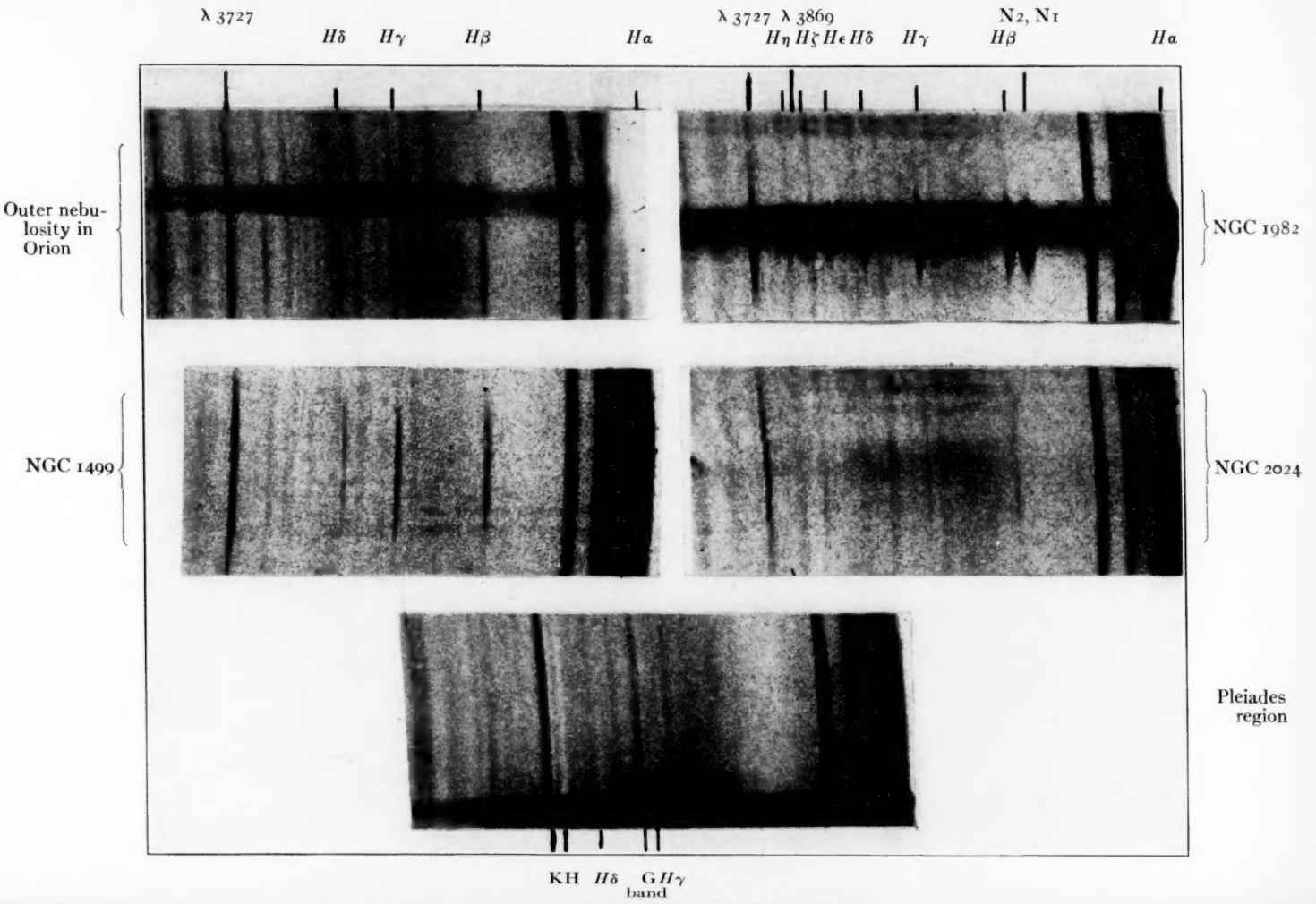

SOME NEW SPECTRA OF GALACTIC NEBULAE

In a recent note[1] a preliminary report was made on the spectra of some diffuse nebulae. We have now obtained a number of new spectrograms (Pl. II) which reveal several features of the problem of nebular excitation.

Perhaps the most interesting is the spectrum of the brightest part of the "Great Spiral" in Orion, the large diffuse nebula which extends through most of the constellation. The slit was centered at α 5^h45^m, $\delta + 0°.8$, and covers $2°$ in right ascension. The plate shows *Hα*, *Hβ*, *Hγ*, *Hδ*, and λ 3727 of [*O* II]. A defect mars the *Hα* region of the negative, but another plate shows *Hα* to be very strong and confirms all other features.[2] The relative weakness of λ 3727 suggests that the nebula is of low excitation—perhaps even lower than the nebulae near γ Cygni. The emission character and the large extent of this nebula, which is at least $3°.5$ from any bright star, mark it as unusual. If it is assumed that the Orion cluster of B stars is the source of luminosity, we can estimate that the linear distance of the nebula from the illuminating source is at least 20 parsecs, and it may be much greater.

The next spectrum, that of the nebula near ξ Persei (NGC 1499), is a typical low-excitation emission nebula. The lines visible are *Hα*, *Hβ*, *Hγ*, *Hδ*, *Hε*, and λ 3727; the nebular lines are weak or absent, even though the exciting star is of type O7 and is of intermediate luminosity. The spectrum of NGC 1982, the detached knot of nebulosity 8′ north of the Trapezium in Orion, is that of a high-excitation nebula in which N1 and N2 of [*O* III] are very strong. The visible lines include *Hα* to *Hκ*, N1 and N2, λ 3727 and λ 3869. The line λ 3869 of [*Ne* III] is strongly concentrated at the center of a continuous spectrum, the source of which is doubtful and is in part the B8 star near the center of the nebula. A spectrum of the Orion nebula at the Trapezium, NGC 1976, does not show the line at λ 3869 but is otherwise similar. It is interesting to make a comparison of the North America nebula, excited by α Cygni (A2p), the Orion nebula, excited by the Trapezium (O6–O9) and NGC 1499,

[1] Greenstein and Henyey, *Ap. J.*, **86**, 620 1937.

[2] We have since obtained a spectrum centered at α 5^h50^m, $\delta -3°$. The emission features are similar, though the nebula is fainter.

excited by ξ Persei (O7). The level of excitation in the North America nebula is very close to that in the Orion nebula, even though the exciting star is of considerably later spectral type; the nebula near ξ Persei is of much lower excitation even though the illuminating star is of early type. This emphasizes the fact that the spectral type of the illuminating star is not the sole determining factor in nebular excitation.

The spectrum of NGC 2024, north of and following ζ Orionis, (Bo), shows what is probably a composite spectrum with an unusual change of the relative intensity of the emission lines along the slit. $H\alpha$ is particularly strong in NGC 2024, on the east, but λ 3727 is enhanced toward the west, where a faint extension of IC 434 is found.

We find that the Balmer decrement is subject to surprising variations. For example, the nebula IC 2159, surrounding the cluster NGC 2175 and excited by an O6 star, shows the hydrogen lines, N1 and λ 3727. A similar spectrum is found for a large nebula near S Monocerotis, spectral type O7s. The excitation as indicated by the strength of N1 is the same. Nevertheless, $H\alpha$ is relatively much stronger in IC 2159—a fact which is corroborated by the great strength of the nebula on direct photographs in the $H\alpha$ region, taken by Struve.[3]

The spectrum of the Pleiades region was obtained south of and preceding Merope. The strong continuous spectrum is partly that of Merope and partly of nebular origin. An absorption line spectrum extends toward the west for 2°, far beyond the usually photographed Pleiades nebulosity. Its character gradually changes with increasing distance from Merope, from a spectrum of early type to one of later type, since the hydrogen lines $H\gamma$ and $H\delta$ are strongest near Merope, while the H and K lines and the G band gain in relative intensity at larger distances. The same result is given by measurement of the energy distribution in the continuous spectrum which shows a change from color class a5 to g5. The early-type spectrum must arise from the scattered radiation from Merope, but the late-type spectrum resembles the normal spectrum of the night sky.

JESSE L. GREENSTEIN[4]
L. G. HENYEY

YERKES OBSERVATORY

[3] *Ap. J.* **86**, 94, 1937.

[4] *National Research Fellow.*